Applied Energy 401 (2025) 126698

Contents lists available at ScienceDirect

Applied Energy

journal homepage: www.elsevier.com/locate/apenergy

Innovative approach and numerical modeling to retrofit existing substations for bidirectional operation: Enabling thermal prosumer participation in District Heating Network☆

Federico Gianaroli [a,*], Mattia Ricci [a], Paolo Sdringola [a], Mauro Pipiciello [b], Diego Menegon [b], Francesco Melino [c]

[a] Italian National Agency for New Technologies, Energy and Sustainable Economic Development (ENEA), Energy Efficiency Department Research Center Casaccia, Via Anguillarese 301, 00123 Rome, Italy
[b] Eurac Research, Institute for Renewable Energy, Viale Druso 1, Bolzano 39100, Italy
[c] Alma Mater Studiorum University of Bologna, Department of Industrial Engineering, Viale Del Risorgimento 2, Bologna 40136, Italy

HIGHLIGHTS

- Bidirectional substations for thermal prosumer integration in district heating networks.
- Retrofit design for bidirectional heat exchange in an existing district heating substation.
- Numerical modeling and simulations assess to the setup under real operating conditions.
- Temporal mismatch limits self-consumption to 10.6 % (mid-season) and 6.2 % (summer).
- The bidirectional setup achieves 94 % useful use of solar energy during summer.

GRAPHICAL ABSTRACT

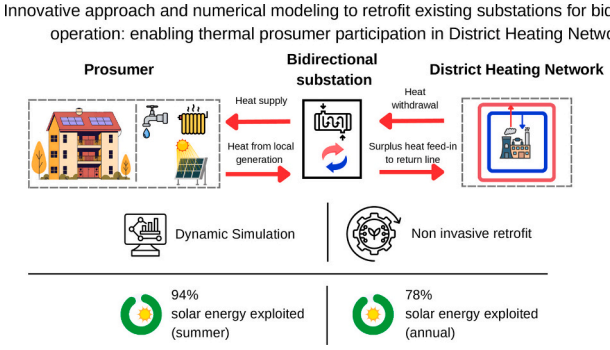

ARTICLE INFO

Keywords:
Bidirectional substation
District heating
Dynamic condition
Modelica language
Thermal prosumer

ABSTRACT

The heating and cooling sector accounts for nearly half of Europe's total energy consumption, highlighting the urgency of its decarbonization. District heating networks, which serve approximately 100 million people across Europe, are recognized by the recent European Energy Efficiency Directives as key infrastructures for integrating renewable energy and waste heat. In Italy, while energy efficiency improvements have primarily focused on thermal production plants, decentralized substations still require upgrades to enhance their performance and support the emergence of thermal prosumers. This study presents a non-invasive retrofit design for an existing substation in a district heating network in Italy, aimed at preserving the integrity of the original infrastructure while implementing a new control system to recover unused solar energy in a supply-to-return configuration. Modelica language and Dymola software are used to develop the numerical model of the bidirectional substation, and multi-domain simulations based on real thermal load and solar production data from a multifamily building are performed with a one-second time step to dynamically test the entire system. Results show that the control

☆ This article is part of a Special issue entitled: 'ICAE 2024(Y.Y)' published in Applied Energy.

* Corresponding author.
E-mail address: federico.gianaroli@enea.it (F. Gianaroli).

https://doi.org/10.1016/j.apenergy.2025.126698
Received 30 April 2025; Received in revised form 25 July 2025; Accepted 30 August 2025
Available online 15 September 2025

strategy effectively manages thermal exchange dynamics even under fluctuating loads. Despite a limited match between solar production and hot water demand, resulting in low self-consumption rates (10.6 % in mid-season and 6.2 % in summer), the bidirectional setup enabled 94 % of the solar energy to be effectively utilized during the summer day. In line with the results obtained for the representative days, the annual extrapolation shows that the proposed configuration enables 78.4 % of the solar energy to be effectively utilized, with a self-sufficiency rate of 32.5 % and a self-consumption rate of 14.9 %. The proposed solution offers a replicable and efficient approach to support the integration of distributed renewable heat sources in existing district heating systems.

Nomenclature

CHP	Combined Heat and Power
DG	Distributed Generation
DH	District Heating
DHN	District Heating Network
DHW	Domestic Hot Water
FMU	Functional Mock up Unit
HE	Heat Exchanger
HIL	Hardware In the Loop
HPC	High Performance Computer
RES	Renewable Energy Sources
SH	Space Heating
STC	Solar Thermal Collector
WHR	Waste Heat Recovery
E	Thermal Energy
S_S	Coefficient of energy self-sufficiency
S_C	Coefficient of self-consumption
U_{ec}	Useful energy coefficient

1. Introduction

1.1. Background

Achieving climate neutrality by 2050, including the interim target of a 55 % reduction in greenhouse gas emissions by 2030, is a central pillar of the European Union's energy and climate strategy, as established by the European Climate Law [1]. Meeting these ambitious goals requires profound transformation across all energy-consuming sectors, with particular emphasis on enhancing energy efficiency, deploying renewable energy sources (RES), and decarbonizing thermal energy systems [2]. Within this context, the heating and cooling sector emerges as a critical challenge: it represents nearly half of Europe's total final energy demand, surpassing the combined consumption of transportation fuels and electricity [3]. Despite technological advances, fossil fuels remain the main source for heating globally, with RES accounting for only 24.8 % of the total heat production as of 2022 [4]. The revised Energy Efficiency Directive (EU/2023/1791) strengthens the European Union's commitment to improving energy performance across all sectors, with a particular focus on promoting efficient district heating (DH) systems. The Directive, aligned with the objectives of the 2021 European Green Deal, emphasizes the reduction of primary energy consumption and the integration of RES and waste heat (WH) into thermal networks [5]. In this context, district heating networks (DHN) are recognized as a key solution for supporting the energy transition, especially in urban areas where decentralized energy production often encounters technical and spatial barriers [6,7].

Europe currently counts approximately 6000 district heating and cooling systems across 32 countries, providing thermal energy to about 100 million people. The highest penetration is found in Scandinavian countries, followed by Germany, France, the United Kingdom, and the Netherlands [8].

In Italy, as of December 2023, there were 434 operational DHN, 152 of which are classified as small or very small systems, mainly concentrated in the northern regions and primarily serving residential needs for space heating (SH) and domestic hot water (DHW). Despite the relatively mature infrastructure, growth in DH in Italy remains modest. According to data provided by AIRU (the Italian District Heating Association) [9], since 2018, the annual increase in heated building volume has remained below 3 %, reaching only 1.7 % in 2023. Similarly, the expansion of the network infrastructure shows a consistent slowdown, with an annual extension of just 97 km in 2023. These trends clearly point to the strategic importance of upgrading and optimizing existing networks, rather than relying on the deployment of new ones, whose growth remains limited. Integrating renewable energy sources into existing systems could play a key role in improving their efficiency, and there is significant potential for progress. Currently, only 2.9 % of the thermal energy directly supplied from renewables, primarily integrated at central production plants, limiting the potential of distributed renewable contributions. In particular, decentralized substations, which represent critical nodes in the network, remain passive infrastructures, with no active role in utilizing locally produced renewable heat.

In this scenario, the concept of decentralization is gaining increasing attention, as both electricity systems and, more recently, DHN seek to enhance flexibility and sustainability by promoting the active participation of distributed producers and prosumers. The transition towards thermal prosumers (i.e. users capable not only of consuming but also of producing and sharing heat with the network) offers significant potential for enhancing the efficiency and RES integration of DHN. At the European level, the Renewable Energy Directive (RED II) [10] provides a clear framework supporting renewable-based energy communities, including thermal energy sharing. However, as highlighted by Gianaroli et al. [11] in a recent work, the majority of initiatives and research efforts have so far concentrated on electricity-based energy communities, while experiences involving thermal prosumers remain limited [12]. By enabling bidirectional thermal energy exchanges and upgrading conventional substations from passive receivers into active units, DHN can evolve towards more decentralized and community-driven energy models, unlocking new opportunities for decarbonization and system flexibility. Within this framework, the present paper explores how to enable heat consumers in Italian district heating systems to act as prosumers by feeding surplus thermal energy into the network.

1.2. Literature review

This section provides an overview of recent literature on the integration of thermal prosumers into DH systems, highlighting different research approaches and areas of focus. In recent years, the scientific community has shown increasing interest in the integration of thermal prosumers within DHN, focusing particularly on the joint modeling of networks and active users, and assessing the impact of prosumers on hydraulic, thermal, and overall energy performance. Since simulation modeling represents the most commonly adopted methodology for these analyses, a dedicated summary is provided in Table 1 to synthetically compare the key characteristics of the most relevant modeling-based studies.

Ancona et al. [13] analyzed the integration of thermal prosumers into a real DHN using the in-house–developed software IHENA, evaluating the impact on hydraulic and thermal parameters as a function of

prosumer location. Similarly, Dattilo et al. [12] employed IHENA to investigate the dynamic behavior of bidirectional networks, analyzing the impact of thermal energy sharing through allocation algorithms developed by Gianaroli et al. [14]. In both cases, the prosumer is modeled as a generic feed-in node, and the simulations are performed under steady-state conditions.

In the context of multi-level dynamic simulation, Bachmann et al. [15] introduced dhcSim, a Modelica-based library specifically designed for complex thermal networks, later adopted by Stanica et al. [16] to simulate a district heating and cooling network integrating RES and thermal prosumers. Testasecca et al. [17] used TRNSYS to model and simulate a low-temperature DHN that combines traditional consumers and prosumers, the latter represented by hotel and apartment buildings equipped with heat pumps, allowing thermal energy to be fed into the network. Brand et al. [18] and Brange et al. [19] both employed NetSim to analyze the integration of thermal prosumers, focusing respectively on decentralized solar thermal collectors (STC) and waste heat recovery (WHR) from buildings with cooling demand, and assessing their impact on network performance and environmental benefits. More recently, Dibos et al. [20] developed HeatNetSim, an open-source tool for simulating future thermal networks with bidirectional flows, using WHR from High Performance Computer (HPC) as a decentralized prosumer source. Lickleder et al. [21] proposed a steady-state thermohydraulic model for smart thermal grids with prosumer integration represented by a generic feed-in node. Gross et al. [22] developed a thermo-hydraulic model to simulate bidirectional DHNs with prosumers, represented by supermarkets with WHR and STC feeding their full output into the network. Kauko et al. and Wang et al. [23,24] both modeled DHNs with decentralized thermal prosumers, including data centers, supermarket, and STC. While [23] adopted a dynamic simulation approach using Dymola/Modelica on a Norwegian case study, [24] used a steady-state Matlab model to assess the integration of STC feeding excess heat into the network. Finally, Lichtenegger et al. [25] focused more on informational and economic aspects, introducing the concept of dynamic heat pricing as a mechanism for autonomous prosumer management.

While previous studies have mainly focused on the system-level impact of prosumers in DHN, examining network performance, energy flows, and thermal or hydraulic behavior, the modeling of individual prosumer substations has received comparatively less attention. However, some works have started to explore this topic in more detail, offering deeper insights into control strategies, operating schemes, and integration methods at the substation level. At the design level, Martinazzoli et al. [26] presented a detailed design of a bidirectional substation prototype for 5GDHN applications, supported by preliminary performance assessments. Sdringola et al. [27] developed a dynamic model of the bidirectional substation in Dymola, based on experimental results obtained in [28]. Dino et al. [29] used TRNSYS to model and simulate the same substation dynamically, extending the analysis to two locations with different solar irradiance profiles. Finally, Zinsmeister et al. [30] explored various prosumer-side configurations using SimulationX to maximize heat exchange efficiency and improve network integration.

Other studies have focused on the analysis of substations designed for thermal prosumers, adopting an experimental approach. Rosemann et al. [31] introduced a dynamic control strategy for DHN substations, validated through Hardware-In-The-Loop (HIL) testing, representing one of the first practical implementations of prosumer substations. Building on initial work on bidirectional substations conducted by Lamaison et al. [32], the same research group tested a bidirectional substation prototype connected to a real DHN through an HIL setup, analyzing data collected over twelve days of operation [33]. Pipiciello et al. [28] developed a first prototype of a bidirectional substation for conventional DHN, validating its feasibility through HIL testing. Subsequently, Pipiciello et al. [34] extended this work by evaluating, over an annual cycle, the contribution of the bidirectional substation to optimizing the use of locally produced thermal energy and its recovery in a high-density urban area. Sdringola et al. [35] further evolved the prototype, not only analyzing the ability of prosumers to feed excess energy into the network but also implementing technical strategies aimed at increasing the local self-consumption of produced thermal energy.

1.3. Aim

The complexity of physically intervening in existing DHN makes simulation-based modeling the most widely adopted approach for studying the integration of thermal prosumers. However, as highlighted in the literature review, most modeling studies focus on the overall interaction between prosumers and the network, often overlooking critical aspects related to the practical feasibility of bidirectional operation. In particular, some main research gaps can be identified:

- Thermal prosumers are often represented as simple nodes that feed or withdraw heat, without accounting for the internal dynamics of the substation, operational constraints, or user behavior that influence real performance.
- Heat feed-in the network is commonly assumed to derive from low-temperature WHR, which limits the applicability of these models to existing networks operating at higher supply temperatures.
- Few studies investigate technically detailed and replicable retrofit strategies that can realistically be implemented in existing DHN, while most models remain confined to theoretical validation.
- None of the reviewed studies addresses the direct engagement of citizens as active participants in the energy management of the network, unlike what has already been explored in the electrical sector with PV citizen prosumers.

To address the research gaps highlighted in the literature, this study

Table 1
Modeling-based studies on thermal prosumer integration in district heating.

Publication	Environment	Prosumer type	DH temperature	Location	Model type
[12,13]	IHENA	General feed-in node	Not specified	Italy	Steady-state
[15,16]	Modelica	General feed-in node	Multilevel network	General	Dynamic
[17]	TRNSYS	Hotel and apartment with HP	60 °C–45 °C (or 50 °C)	Italy	Dynamic
[18]	NetSim and WinSun	Decentralized source with STC	Seasonal trend	Sweden	Steady-state and Dynamic
[19]	NetSim	WHR from space cooling	65 °C–30 °C	Sweden	Steady-state
[20]	HeatNetSim and Modelica	WHR from HPC	30 °C–20 °C	Germany	Quasi-dynamic
[21]	ProHeatNet_Sim	General feed-in node	65 °C–42 °C (or 52 °C)	General	Steady-state
[22]	C#.NET language and TRNSYS	WHR (supermarket) and STC (residential)	20 °C (ULTDH)	Germany	Steady-state
[23]	Dymola Modelica	WHR from datacentre and supermarket	65 °C–45 °C	Norway	Dynamic
[24]	Matlab, CESAR and ArcGIS	STC from residential	70 °C–30 °C	Switzerland	Steady-state
[27]	Dymola Modelica	General DG	80 °C–60 °C	Italy	Dynamic
[29]	TRNSYS	STC	80 °C–50 °C	Italy and Germany	Dynamic
[30]	SimulationX	Multiple scenarios (Boilers, HP, STC)	65 °C–45 °C or 40 °C–30 °C	General	Dynamic

presents a detailed numerical modeling of a bidirectional substation designed to convert a residential citizen into a thermal prosumer through a non-invasive retrofit solution.

The present work is based on a real case study, taken from an existing DHN in the city of Turin (Northern Italy), whose configuration is representative of many similar networks in Italy. Specific technical and design constraints from the real context were considered to ensure that the proposed solution remains replicable without requiring invasive interventions on the infrastructure.

Before applying the concept to the real network, an existing experimental prototype of a substation, previously validated in experimental campaigns [28,34,35], was modified to faithfully reproduce the intended retrofit configuration.

A dynamic model of the substation was then developed in Dymola, using experimental data from the prototype as input, combined with solar production and heat demand profiles from a multi-family residential building.

The model simulates the system behavior with high temporal resolution, using a one-second time step, over a set of representative days for each season, enabling an in-depth evaluation of the control logic and system dynamics during transitions between feed-in and withdrawal modes.

Building on this modeling framework, the present work offers concrete contributions that directly address the gaps identified in the literature. These key points, previously outlined in the discussion, are summarized as follows:

- The integration of thermal prosumers through bidirectional substations remains largely unexplored, with most studies focusing on system-level modeling.
- The non-invasive retrofit approach introduces a novel perspective by focusing on the adaptation of existing substations rather than designing entirely new systems.
- The case study is representative and highly replicable, while also fostering citizen engagement by enabling users to become thermal prosumers.
- The high-resolution dynamic simulation enables accurate evaluation of system performance under realistic conditions, while also providing a component that can be directly integrated into DHN models in Dymola, OpenModelica, or exported as Functional Mock-up Unit (FMU) for use in other simulation platforms.
- The work presents a comprehensive and multidisciplinary approach, covering the identification of a relevant case study, the design of the retrofit intervention, and the development of a detailed numerical model.

In summary, this study provides a significant advancement to the existing literature by proposing innovative strategies for enhancing the performance of existing substations and facilitating the integration of thermal prosumers.

1.4. Paper structure

To address the research gaps highlighted in Section 1.3, the paper is structured as follows. Section 2 illustrates the adopted methodology: Section 2.1 introduces the reference DHN and the existing substation analyzed in the study; Section 2.2 presents the retrofit intervention designed to enable bidirectional operation. Section 2.3 describes the numerical model developed in Dymola, including its main components and control logic. Section 2.4 provides details on the simulation setup, the selection of representative seasonal days, and the experimental prototype used to generate the input data. Section 3 presents the simulation results. Section 3.1 analyzes the key dynamic variables to assess the behavior of the bidirectional substation. Section 3.2 focuses on the daily energy exchanges, while Section 3.3 extends the analysis to an annual scale through data extrapolation. Finally, Section 4 summarizes the key conclusions derived from the modifications applied to the system.

2. Materials and methods

2.1. DHN case study

In recent years, in Italy, rather than focusing on the design of new DHN, a key aspect of DH decarbonization has been the improvement of existing infrastructures. Efforts to improve the energy efficiency of existing DHN and integrate RES into operational systems focus on developing flexible solutions that can be easily replicated in other contexts. Given the goal of proposing a retrofit project for existing substations, as part of the research activities within the Implementation Plan 2022–2024 of the Italian Programme known as *Electric System Research*, a specific DHN has been selected for detailed analysis.

The selected DHN supplies thermal energy to 34 residential buildings located in Turin, a city in Northern Italy. Each building is equipped with an individual substation featuring heat exchangers that provide energy for both SH and DHW production. The network's supply temperature is set at 80 °C during the thermal season, and reduced to 70 °C in summer, while the return temperatures are 60 °C and 50 °C respectively, maintaining a temperature differential (ΔT) of 20 °C. The DHN operates with a two-pipe configuration, commonly used in residential and tertiary networks: one pipe provides thermal energy for SH and DHW to the substations, while the other returns the cooled fluid to the heat generation plant. Fig. A1 in the Appendix A presents a schematic overview of the DHN, which extents for just over one kilometre north of the city. The network is powered by a combined heat and power (CHP) plant, which includes an internal combustion engine and two boilers, utilizing hot water as the heat transfer medium. The total installed thermal power at the plant is just under 11.2 MW, with an average thermal efficiency of 73.20 %. The system has a branched structure with multiple distribution points. The main pipeline has a diameter of DN250, while the majority of the connection pipes measure DN60.

In order to cover the thermal demand for DHW, flat-plate solar collectors (efficiency 82 %, forced circulation) were installed in 16 residential buildings across the network, collectively housing 652 dwellings: 10 users are equipped with 30 solar collectors, southeast oriented, 30° tilt angle, covering 77 m2; the remaining 6 are equipped with 36 solar collectors, east oriented, 30° tilt angle, covering 92 m2. This paper focuses on the analysis of a specific substation within the network, featuring a heat exchanger (HE1 400 kW) designed to facilitate thermal energy transfer between the district heating system and the end user (seven-story building comprising 42 housing units). In its current configuration, the heat exchanger serves both SH and DHW demands, reaching 366 kW. Additionally, the substation includes a thermal storage system comprising five dedicated tanks exclusively used for DHW for overall 5000 l. A photograph of the analyzed substation is shown in Fig. 1.

A part of the thermal load for DHW is supplied by solar energy generated from flat-plate collectors installed on the building's rooftop, which feed the heat exchanger located at the bottom of the thermal storage tanks (HE2, 130 kW). When solar radiation is insufficient to heat the water, the DHN provides the additional thermal energy needed to achieve the desired storage temperature. Fig. 2 presents a simplified schematic of the substation currently integrated into the DHN in Turin, highlighting only the essential components involved in the interaction between the DHN and the end user. The diagram outlines three main circuits:

- The primary circuit, connected to the DHN's supply (red) and return (blue) pipelines, transfers heat from the main network to the secondary circuit via HE1, meeting the user's thermal load.

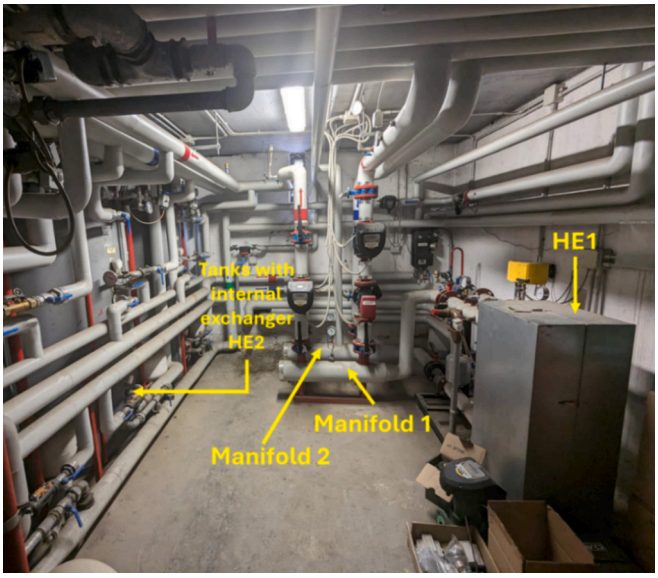

Fig. 1. Photograph of the analyzed substation.

- The secondary circuit facilitates the transfer of heat from HE1 to the user's SH system and the upper heat exchanger of the DHW storage tank.
- The tertiary circuit enables the transfer of thermal energy from local solar production to the lower heat exchanger of the DHW storage tank (HE2).

The substation control is achieved through a thermo-electric system based on flow, managed by valves and circulators in the various circuits.

The existing V1 valve fully opens (on/off) if:

- It is between 6 AM and 10 PM during the heating season (October 15 to April 15)
- Storage temperature (T_{tank}) < 60 °C

The existing V3 valve fully opens (on/off) if:

- T_{tank} < 60 °C and solar temperature (T_5) > T_{tank} + ΔT (5 °C)

Additionally, the Psh pump ensures circulation throughout the entire heating season, facilitating the continuous flow of thermal power. Temperature regulation for space heating is achieved through a mixing valve, which is not shown in the schematic substation. Furthermore, the Pdhw pump is responsible for circulating the flow to the upper heat exchanger of the tank, when the tank temperature falls below its nominal value.

2.2. Retrofit design

To enable bidirectional exchange with the existing substation and the DHN without disrupting its original configuration, this retrofit has been designed to be fully non-invasive. Indeed, the primary goal was to preserve the operational integrity and performance of the system, ensuring that the original heat distribution processes remained unaltered. Rather than modifying the core functionality, the retrofit introduces an additional operational layer that optimizes energy usage and allows for greater integration of renewables, while keeping the existing control logic intact. In achieving this, several key constraints were carefully considered in accordance with the network operator's directives:

- Inaccessibility of the main DHN branch, confining all interventions to the existing infrastructure.
- Limited space within the substation technical room, requiring compact solutions that do not interfere with current equipment.
- Preservation of the existing valve control logic, meaning the retrofit could not interfere with the pre-established control routines, ensuring seamless system operation.

In 2021, a study from Pipiciello et al. [28] analyzed various configurations for prosumer substations and identified the return-to-supply option as the best solution for facilitating the integration of RES and improving system efficiency. However, despite the theoretical advantages of this configuration, the final choice for the retrofit of the existing substation was the supply-to-return. This decision was driven by several constraints related to the existing infrastructure and control logic of the substation.

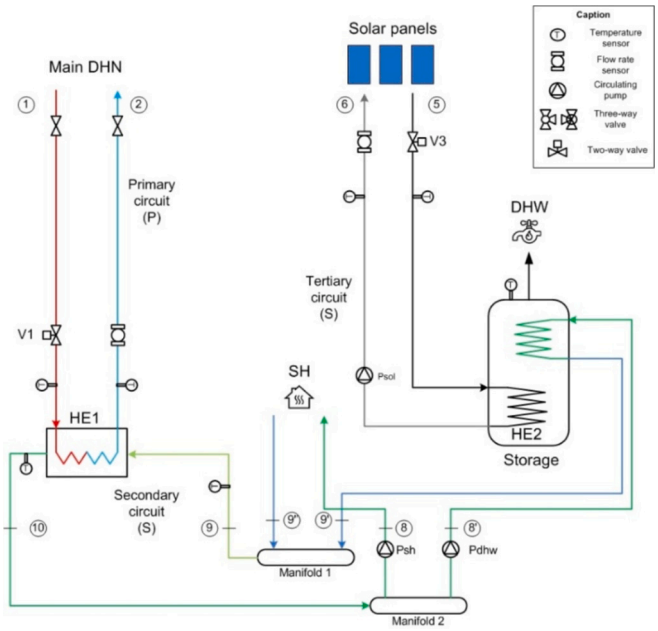

Fig. 2. Layout of the existing thermal substation.

In particular, the V1 valve, which regulates flow on the supply side, prevents the flow from passing through the return branch unless there is a heating or domestic hot water (DHW) demand. This could occur when excess solar heat is produced, preventing the utilization of this useful energy. Additionally, due to the inaccessibility of the main district heating network (DHN) branch and space limitations in the substation room, making modifications that would require disconnections or complex interventions—such as those needed for a return-to-supply configuration—was not an option. Given these considerations, the supply-to-return configuration was selected as the optimal solution for the retrofit. This configuration allows excess solar energy to be effectively fed into the DHN without disrupting the existing control logic and without requiring intrusive changes to the main network.

Fig. 3 illustrates the updated substation layout, highlighting the retrofit components in purple. A key feature of the new design is the integration of an additional heat exchanger in a supply-to-return configuration (HE3, 65 kW at design conditions in this specific substation, thermal exchange efficiency 75 %). At HE3, the fluid is taken from the primary loop flow line, exchanges heat with the solar collectors and is reintroduced into the return line at a higher temperature. This configuration allows the substation to utilize excess heat energy, produced when the solar collectors generate more heat than is required for DHW, in the DHN. The retrofit improves system efficiency and facilitates the integration of renewable energy without compromising the stability and control logic of the original system.

Compared to the unidirectional configuration (Fig. 2), the installation of new valves and the implementation of new control strategies have been proposed. The new V2 valve regulates the flow from the supply branch of primary circuit to HE1, based on the temperature in section 10. This is done in order to maintain a constant value of the supply temperature ($T_{10} = T_{10,obj}$) through a PI control. In detail:

- if $T_{10} > T_{10,obj}$, it diverts the fluid, bypassing HE1;
- if $T_{10} < T_{10,obj}$, valve V2 increases the flow sent to HE1;
- if $T_{10} = T_{10,obj}$, valve V2 maintains its current opening position;
- if valve V1 is closed, then V2 does not work.

The new control logic of the tertiary circuit is schematized in Fig. 4 and is based on several conditions related to solar production and system temperature. When solar production is available, the system controls if the solar temperature exceeds tank temperature and if the tank temperature is below the defined set point value. If both conditions are met, the V3 valve opens, allowing the flow into the tank. If either condition is not met, but the solar temperature still exceeds the supply temperature of the network, the V3 valve opens and the V4 valve bypasses the tank. Subsequently, through further control, the flow is directed to the HE3 heat exchanger for injection into the network via V5 and V6. Additionally, to prevent rapid switching of the valves, a hysteresis of 2 °C is applied, ensuring stable and efficient operation.

The main challenge of this new configuration lies in testing and fine-tuning the newly implemented control strategies alongside the existing ones, ensuring their proper coordination. In particular, attention must be given to the simultaneity of valve openings, transient behaviours, and the avoidance of undesired cycling of heat exchangers, which could impact the overall system efficiency.

2.3. Numerical modeling

2.3.1. Modeling framework and fundamental components

To test the implemented control strategies and the overall system, a numerical approach has been used to analyze the efficiency and stability of the retrofit solutions. The object-oriented, equation-based programming language Modelica and Dymola software have been employed for multi-domain simulations and model-based design of dynamic systems such as the bidirectional substation. Dymola provides an interactive environment and tools for simulating complex system interactions using a mixed symbolic and numerical solver. As highlighted by Höffner et al. [37], this approach allows for informed decisions on energy management in urban networks without physical modifications to the grid. Additionally, Abugabbara et al. [38] demonstrate the effectiveness of Modelica in simulating low-temperature district heating systems and testing dynamic system behavior.

The modeling of the bidirectional substation has been primarily carried out using two key libraries: the *Modelica Standard Library* and the *IBPSA Library*. The *Modelica Standard Library* is an open-source resource that provides a wide range of components for simulating mechanical, electrical, thermal, and control systems, along with utilities for numerical operations, string management, and file handling. Complementing this, the *IBPSA Library* features over 300 classes specifically tailored for energy and control system modeling. To establish the connections

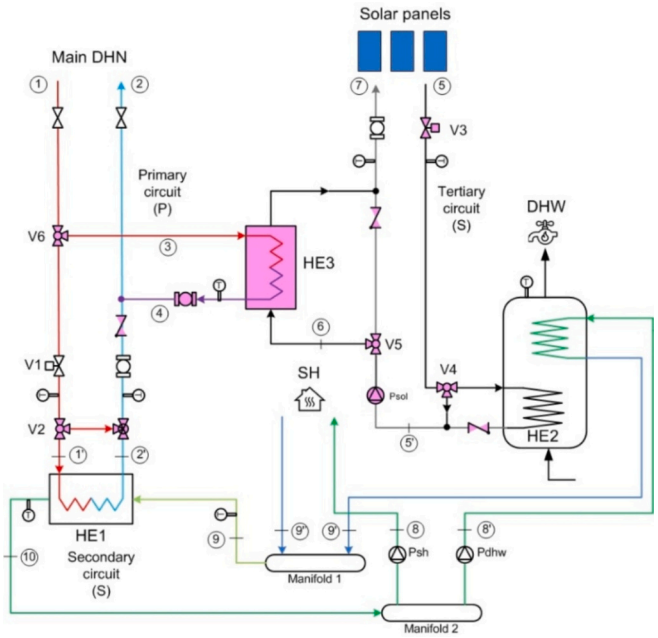

Fig. 3. Layout of the existing thermal substation, in bidirectional configuration.

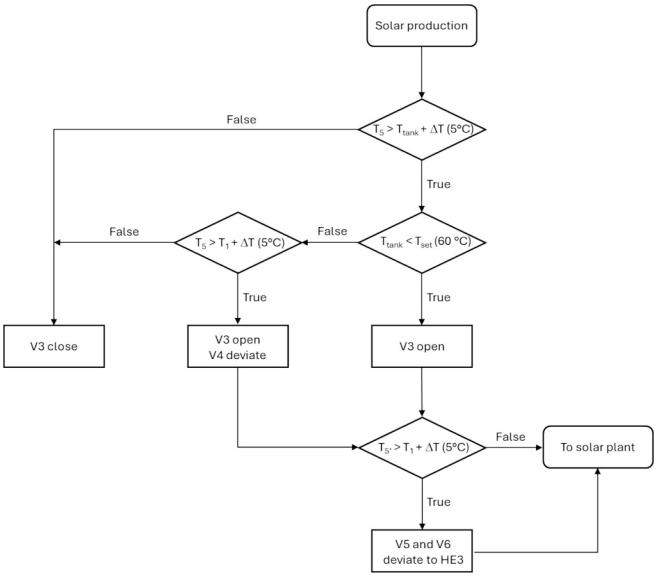

Fig. 4. Flowchart of the new control system of tertiary circuit of bidirectional substation.

between the primary components within the substation, *StaticPipe* models have been used, since due to the limited length of pipes dynamic transient effects can be neglected. Thus, these models represent straight pipes with a uniform cross-section and assume steady-state balances of mass, momentum, and energy, without accounting for mass or energy accumulation. Each port in the fluid system is characterized by two thermodynamic states, and the momentum balance considers factors such as momentum flux, frictional losses, and gravitational effects. For defining boundary conditions, the *MassFlowSource_T* and *Boundary_pT* models have been employed. *MassFlowSource_T* simulates an ideal mass flow source where parameters like flow rate, temperature, fluid composition, and trace substances can be specified. This model allows the mass flow rate to be set as a fixed value or dynamically adjusted through input connectors, enabling interaction with external signals to modulate system behavior. The *Boundary_pT* model is used to define boundary conditions by setting parameters such as pressure, temperature, and fluid composition. These can be applied as fixed values or modified dynamically through external inputs, offering greater flexibility in adapting the model to various scenarios implemented. These boundary conditions affect fluid flow only when it moves outward from the component; if the flow is reversed, they act as passive sinks without influencing the simulation. For sensors, *TemperatureTwoPort* and *MassFlowRate* models were integrated. The *TemperatureTwoPort* sensor was critical for tracking fluid temperature in motion and played a key role in the substation's control logic. Since it is modeled as an ideal sensor, it does not influence the fluid's thermodynamic behavior. The *MassFlowRate* sensor measures the mass flow between fluid ports a and b, and, like the temperature sensor, it operates without altering the system's dynamics.

2.3.2. Heat exchanger

A key component in the development of the bidirectional substation is the heat exchanger, which enables the transfer of thermal energy between different fluid streams. To model this element, the *Constant Effectiveness* model has been employed. This heat exchanger features two inlets and two outlets, operating at a fixed efficiency level and transferring thermal energy based on the principles outlined in Eq. 1. The model is sourced from the *IBPSA Fluid library*, specifically within the *HeatExchanger* sub-package.

$$Q = \varepsilon \bullet Q_{\max} \tag{1}$$

where ε represents the heat exchange efficiency, while Q_{max} represents the maximum transferable thermal power, which occurs when the fluid with the lower thermal capacity reaches the temperature of the fluid with the higher thermal capacity—effectively simulating an infinite heat exchange surface. The thermal power relation is detailed in Eq. 2.

$$Q_{max} = C_{min} \bullet \left(T_{hot_i} - T_{cold_i}\right) \tag{2}$$

where C_{min} (Eq. 5) refers to the smaller value between the hourly thermal capacities of the hot and cold fluids (kW/K), as defined in Eqs. 3 and 4, respectively.

$$C_{hot} = m_{hot} \bullet c_{ph} \tag{3}$$

$$C_{cold} = m_{cold} \bullet c_{pc} \tag{4}$$

$$C_{min} = min(C_{hot}, C_{cold}) \tag{5}$$

where m_{hot} and m_{cold} are the mass flow rates of the hot and cold fluids, respectively (kg/s), and c_{ph} and c_{pc} are the specific heats at constant pressure of the hot and cold fluids, respectively (J/kgK).

2.3.3. Three-way valve

The three-way valves in the substation model are used to divert fluid flow within the primary and tertiary circuits. These valves are modeled using the *ThreeWayValveLinear* component from the *IBPSA library*. As shown in Fig. 5, which illustrates the *ThreeWayValveLinear* model, fluid typically enters through port 1, exits through port 2, and can either enter or exit through port 3. This component can be set to work as a 3-way mixing or diverting valve with linear opening characteristics. To configure the valve in diverting mode, the flow paths were modified by reversing the fluid flow through the ports compared to the standard

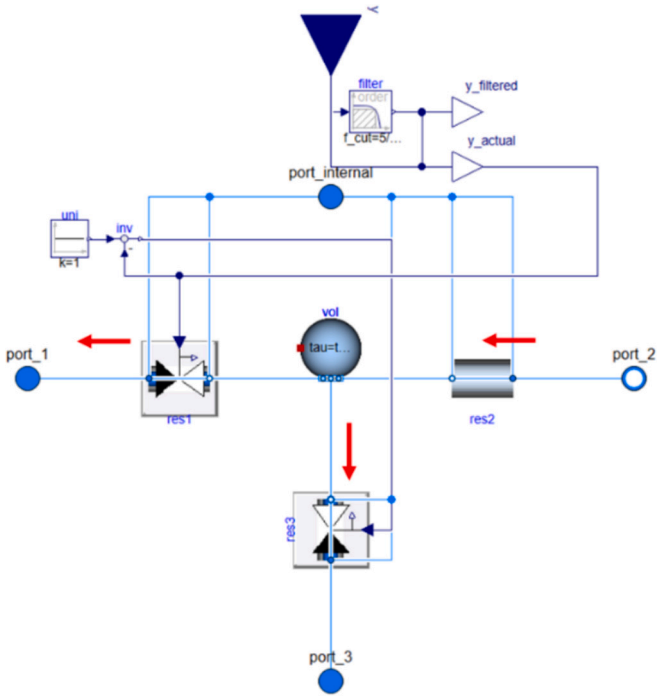

Fig. 5. Three-way valve IBPSA model.

model. Specifically, fluid enters through port 2, passes through res2 (a lossless pipe), and exits either through port 1 or port 3 (please see red arrows shown in Fig. 5). This behavior is controlled by input signals 0 and 1 from the integrated control logic, leveraging the linear opening characteristics of res1 and res3. When the control signal is 1, the flow is directed from port 2 to port 1; when the signal is 0, the flow is diverted from port 2 to port 3.

2.3.4. Controllers

It is widely recognized that a proportional (P) controller applies a correction that scales with the error, governed by the proportional gain K. Increasing K enhances the system's responsiveness, pushing the controller output closer to the reference value. However, due to the inherent steady-state error, the system never fully reaches the setpoint. At the same time, higher values of K can lead to more pronounced oscillations around the target, potentially driving the system towards instability. The integral (I) controller, on the other hand, contributes based on the accumulated error over time effectively responding to the average error. This integration eliminates the steady-state error left by the proportional component. The key parameter here is the integration time constant Ti; a smaller Ti intensifies the integration effect, but also increases the likelihood of oscillations, which may take longer to stabilize. When combined, the proportional and integral actions form the PI controller, which offers a balanced approach by improving accuracy, maintaining system stability, and ensuring a satisfactory response speed. PI controllers are particularly effective in systems characterized by slow changes in load, as they minimize steady-state errors without sacrificing performance. For modeling the substation, PI controllers were implemented using the *Modelica.LimPID* component from the *Modelica.Blocks.Continuous.LimPID* package. In this specific application, the PI controller was used to regulate valve V1', which adjusts the primary circuit flow rate to the HE1 by continuously monitoring the temperature at point T_{10}.

2.3.5. Tank with dual internal exchanger

A crucial component in the design of the bidirectional substation is the storage tank with dual internal heat exchanger. This component plays a key role in producing DHW by facilitating thermal exchange between the tank's stored fluid and either the hot flow supplied by the secondary circuit or the thermal energy generated by the solar collectors. To accurately model this setup, the *StratifiedEnhancedInternalHex* component from the *IBPSA* Fluid sub-library have been used. This model represents a stratified storage tank with an integrated heat exchanger and features fluid ports that enable thermal energy transfer from a circulating heat exchange fluid to the stored water. The heat exchanger operates with an internal helical coil carrying the heat transfer fluid, while the surrounding fluid in the tank remains static, as illustrated in Fig. 6. The model parameters define both the heat transfer characteristics under nominal operating conditions and the geometric properties of the heat exchanger. These inputs are used to calculate the convective heat transfer between the exchanger fluid and the tank's stored fluid.

The positioning of the heat exchanger within the tank is defined by the parameters *hHex_a* and *hHex_b*, which specify the heights of fluid ports a and b relative to the tank's base. These height values also determine *segHex_a* and *segHex_b*, corresponding to the specific tank segments where the heat exchanger ports are connected. Additionally, the model can simulate the dynamic behavior of the heat exchanger by incorporating parameters such as *EnergyDynamicsHexSolid*, *EnergyDynamicsHex*, and *massDynamicsHex*. These parameters provide an approximation of both the fluid volume within the exchanger and the thermal capacity of the heat exchanger wall (*CHex*), both of which are functions of the exchanger's length (*lHex*). The heat exchanger's geometry is modeled under the assumption of a cylindrical steel coil with a diameter equal to half of the tank's diameter, as described in Eq. 6. The length of the heat exchanger is approximated using the relation provided in Eq. 7.

$$\mathrm{rHex} = \frac{\mathrm{rTan}}{2} \tag{6}$$

$$\mathrm{lHex} = 2 \bullet \mathrm{rHex} \bullet \pi \bullet \mathrm{h} \tag{7}$$

where h represents the distance between the inlet and outlet of the heat exchanger. At the core of the structure of the model of the tank implement lies the *StratifiedEnhanced* model, which represents a stratified thermal storage tank segmented into multiple fluid layers, numbered from top to bottom, as depicted in Fig. 6. This model simulates heat

conduction both between the fluid segments and between the tank and its external environment.

The *IBPSA* tank model with a single internal heat exchanger was insufficient for accurately simulating the bidirectional substation, as it did not include a second coil to accommodate supply from the DHN. To address this, a new component was developed, inheriting the same classes as *StratifiedEnhancedInternalHex*, enabling the simultaneous operation of both the solar thermal panels and the DHN for hot water production within the substation model. Specifically, two additional fluid ports, a1 and b1, were introduced to represent the new heat exchanger, *indTanHex1*. This was accomplished by modifying the model's code to define new variables marked with the subscript *1*.

2.3.6. Bidirectional substation model

The dynamic model of the bidirectional substation, designed to operate year-round, is presented in Fig. 7. As previously discussed, all components are either sourced from the *Standard Modelica* and *IBPSA* libraries or custom-built based on elements from these libraries. The colour scheme in the model mirrors that of the substation layout: the primary, secondary, and tertiary circuits are represented with distinct colours, while dashed lines indicate control signals. The dynamic simulations involve varying the DHW demand in terms of both temperature and flow rate, adjusting the space heating service by modifying the return temperature to the secondary circuit, and altering the solar generation profile based on temperature fluctuations. These variations necessitate the implementation of comprehensive control systems to manage the complex interactions between these parameters. In the Dymola model, boundary conditions are dynamically set using a data table as an input signal. This table consists of two columns: the first records time in seconds, while the second specifies the variable values to be adjusted over time.

2.3.7. Control blocks

The control logics were developed based on the descriptions provided in the section 3.2 but adapted to account for the dynamic behavior of the components, with a focus on the substation's operational configuration as defined by the implemented control system. The control strategies have been encapsulated within dedicated control blocks, designed with inputs to receive signals from reference sensors and outputs to transmit signals to the respective valves or sections. The subscripts of the variables used within the control blocks are consistent with those shown in Fig. 4, ensuring clarity and direct correspondence between the control logic and the system layout. Each control block (C1–C4) is described with reference to its specific role in the overall control strategy, the input signals it receives, the logical conditions for activation, and the key functional sub-blocks it includes, such as switches, PID controllers, and hysteresis logic. The associated exploded figures illustrate the internal structure of each block, helping the reader understand the dynamic behavior of the control system and the timing of valve actuation during different operational scenarios.

Control C1. Fig. 8 shows an exploded view of control block C1 and its main components. Block C1 is responsible for the function of valve V1. It receives input data regarding the heating schedule (from October 15 to April 15, between 6:00 AM and 10:00 PM) and the temperature measured at ¾ height of the storage tank. A 2 °C hysteresis range (68–70 °C) is applied to this temperature to reduce significant fluctuations in the water temperature inside the tank. The output of the hysteresis block is inverted using a *NOT* gate, producing a Boolean signal that is true when the tank temperature is below the threshold. In parallel, the seasonal schedule signal (provided as a numeric input) is converted into Boolean format through a *realToBoolean* block. The two Boolean signals are then combined through an OR gate: the output is true if at least one of the two activation conditions is met (tank below setpoint or active heating time window). The *switch* component, present in all control blocks, sets a fixed flow value (y) and activates the valve if the input boolean signal (in pink) is true. Otherwise, it sets $y = 0$, indicating that the valve is closed. This logic is also applied to the SH blocks (without input from the tank) and the DHW blocks (without input from the heating schedule).

Control C2. Fig. 9 shows the exploded view of control block C2, which manages the function of valve V2 for controlling the flow to heat exchanger HE1. The block receives as inputs the flow rate M_1, measured upstream of HE1 and determined by the previous control block C1, and the temperature T_{10} measured at the outlet of HE1.

The flow through HE1 is modulated by a PID controller that adjusts the valve opening based on the deviation between T10 and the reference temperature T10,obj (set to 62 °C). This ensures that the outlet temperature of HE1 remains within the desired range. To prevent the PID controller from operating in the absence of flow (e.g. outside heating hours or when there is no demand from the tank), the control output is disabled and the valve is fully closed. Since a zero value may cause numerical instability in the model, a very small threshold (1e-4) is used to detect near-zero flow conditions. When the flow is above this threshold, the PID controller becomes active and regulates the temperature at T10. As in the other control blocks, a switch component then determines the final output: if the bypass condition is false, the PID output is used to control the valve. Otherwise, the valve is closed. This configuration ensures precise control of outlet temperature under normal flow conditions while avoiding instability when the flow rate is too low.

Control C3. Fig. 10 shows an exploded view of control block C3 and its components. This block manages the function of valve V3. Specifically, if the solar supply temperature (T_5) exceeds the tank temperature (T_{tank}) by more than 5 °C and the water temperature in the tank is below the setpoint (60 °C), or if the solar supply temperature (T_5) is higher than the district heating supply temperature (T_1) by more than 5 °C, the

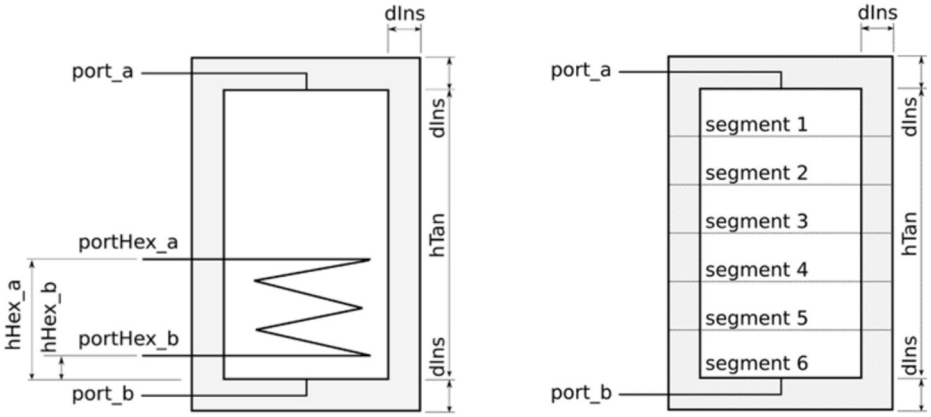

Fig. 6. *StratifiedEnhancedInternalHex* layout (a) and *StratifiedEnhancedInternalHex* layout segmentation (b) [39].

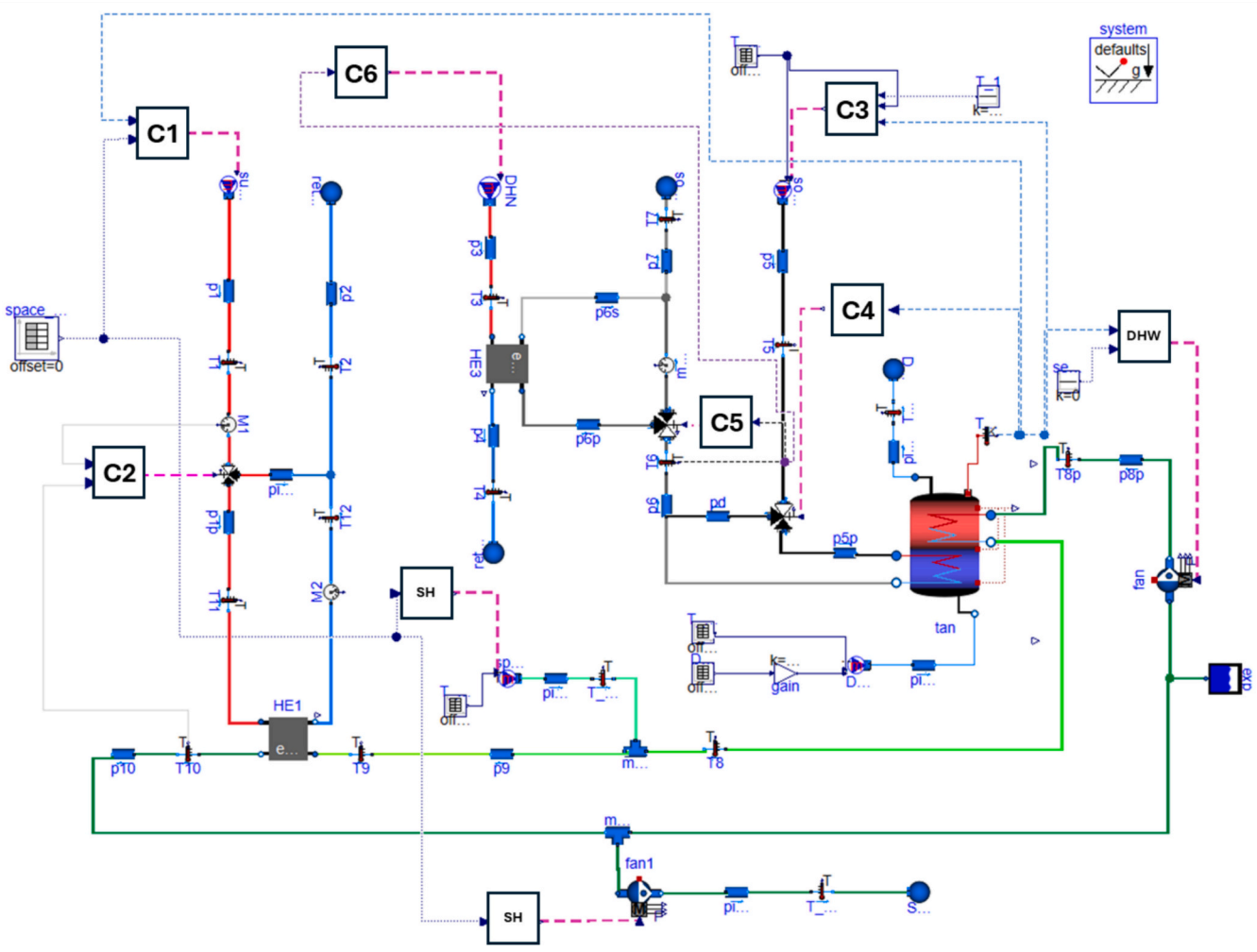

Fig. 7. Bidirectional substation Dymola model.

nominal flow is extracted from the tertiary circuit by opening the valve through the switch. The different conditions are processed separately and then combined using a logical OR gate. If either of them is satisfied, the switch component sets the output flow to a nominal value of 0.85, allowing the system to take advantage of the available solar energy. Otherwise, the flow is set to zero, and the valve remains closed.

Control C4. Fig. 11 shows an exploded view of control block C4, illustrating the key components involved. This block sends a signal to the three-way valve V4, which redirects the flow to bypass the storage tank once the tank has reached the setpoint temperature.

The logic is based on the tank temperature signal, which is processed through the same hysteresis block of C1 to avoid frequent switching around the threshold. The output of the hysteresis is inverted, so that when the tank temperature is below the threshold, the flow is directed into the tank. When the tank reaches or exceeds the upper limit, the signal switches and the flow is redirected through the bypass. The switch

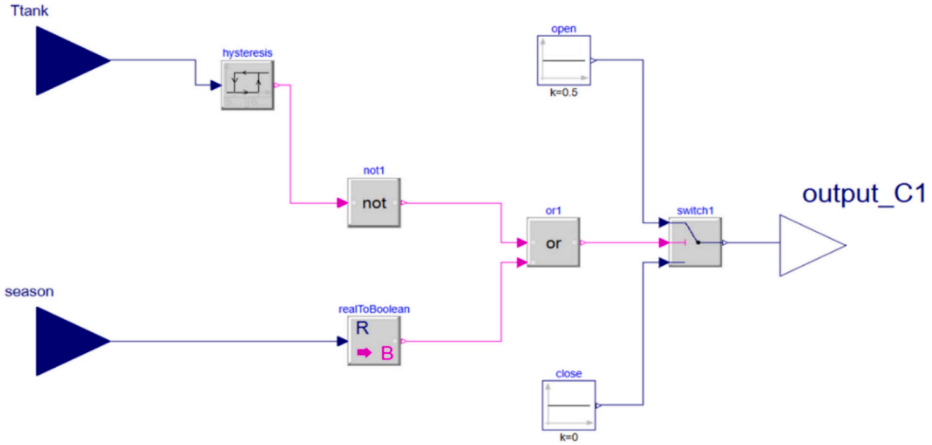

Fig. 8. C1 control block.

component generates the corresponding output signal, setting it to one when flow should go to the tank, and to zero when it should be diverted. The same logic, although with different inputs and outputs, was applied to control blocks C5 and C6, which direct flow to heat exchanger HE3 for feed into the network when the temperature measured downstream of the solar-tank heat exchanger exceeds the supply temperature of the network by a ΔT of 5 °C. The network supply temperature is set to 80 °C during the heating season and 70 °C outside the heating season.

The management of the control strategies described presents significant challenges due to rapid thermal transients and the need for precise adjustments through PID controllers, which operate on very sensitive parameters. The synchronization of the valves and the simultaneous coordination of the various control blocks are crucial to ensure optimal system performance, avoiding unwanted oscillations and maintaining the overall stability of the district heating network.

2.4. Simulation and performance evaluation methodology

2.4.1. Description of the experimental HIL substation prototype

In order to evaluate the effectiveness of the newly designed configuration for converting a real user into an active prosumer, specific experimental testing campaigns [36] were performed at the Energy Exchange Laboratory of Eurac Research on a prototype of a bidirectional substation [28,34,35], which replicates, at a reduced scale (around 60 kW), the same configuration as the real user installation. The hardware-in-the-loop technique was employed to couple the substation in real time with data-driven profiles representing thermal loads (from a multifamily residential building) and local energy production (from solar panels).

Both the building and the plant components were modeled using the dynamic simulation software TRNSYS; the weather file used for the simulations was obtained from the Meteonorm database [40] and refers to a city in Northern Itay. The building model considered is representative of a standard small Multi-Family House (s-MFH) built in the European Continental climate, as described in [41]. t consists of five floors with two apartments per floor, each with a net area of 50 m^2. In terms of annual building thermal energy demand, the outcomes can be regarded as representative of realistic scenarios, as they have been validated against both statistical and monitored data, as reported in [42]. To accurately simulate the thermal behavior of the apartments without excessively increasing the complexity of the model, each apartment was divided into two thermal zones (day/night), and the heat distribution system was modeled with a single radiator, controlled by thermostatic valves. The supply temperature to the radiators is managed according to a weather-compensated heating curve based on the outdoor temperature. The sizing of the radiators in each apartment was based on peak heating demand, obtained from a full-year simulation of the building, and ranges between 1.9 kW and 3.1 kW per apartment. To realistically simulate the domestic hot water demand, ten DHW demand profiles (one for each apartment) were summed. These apartment profiles are stochastic and were generated using the DHWcalc tool [43]. The installed thermal power for space heating is approximately 45 kW, while the peak load for DHW consumption is about 23 kW.

The solar thermal system has a nominal thermal power approximately equal to that of the bidirectional substation (60 kW). The solar field consists of panels tilted at 45° to improve performance during the heating season and oriented to the South. The system includes 10 collector strings connected in parallel, each composed of 5 panels (nominal efficiency of 61 % [44]), for a total collector surface area of 110 m^2. To properly test the dynamics of the control system, simulations have been conducted with a time step of one second. This interval allows for precise capture of rapid variations in operational variables, such as temperature fluctuations in response to sudden changes in thermal flow or variations in the demand for SH or DHW and enables a correct analysis of the dynamic behavior of the valves and other system components. For further details on the prototype specifications and experimental setup, please refer to [34].

2.4.2. Selection of representative days and simulation conditions

To assess the substation's performance, four non-consecutive days are selected to capture variations in weather conditions, following the procedure described in [45]. These days, previously validated in other studies and derived from the HIL prototype described in Section 2.4.1, provide high-resolution input data (with a time step of one second), which are effective for realistically simulating the substation's dynamic behavior, including rapid transients, thermal fluctuations, and control system responses. The selected days are detailed in Table 2, while Fig. 12 shows the daily solar irradiance profiles. As observed, solar conditions vary significantly: August 1 displays high and smooth irradiance typical of summer, whereas January 5 and November 5 exhibit lower, more irregular patterns, reflecting the greater atmospheric variability in winter and autumn.

Although the detailed analysis focuses on four representative days, this study also aims to evaluate the substation's performance over a full year. For this purpose, an extrapolation method previously validated in the literature [45] was applied, using a total of six selected days. In addition to the four discussed in the present section, two additional days were simulated. Their characteristics and results are reported in Appendix B, as they were included solely to ensure the reliability of the annual extrapolation. This approach enables a robust year-round performance assessment while keeping simulation time reasonable, with an error margin below 10 % compared to a full hourly simulation. Eq. 8 shows the formulation for annual extrapolation.

$$Q_{annual=} \sum_{i=1}^{6} Q_i \bullet N_i \tag{8}$$

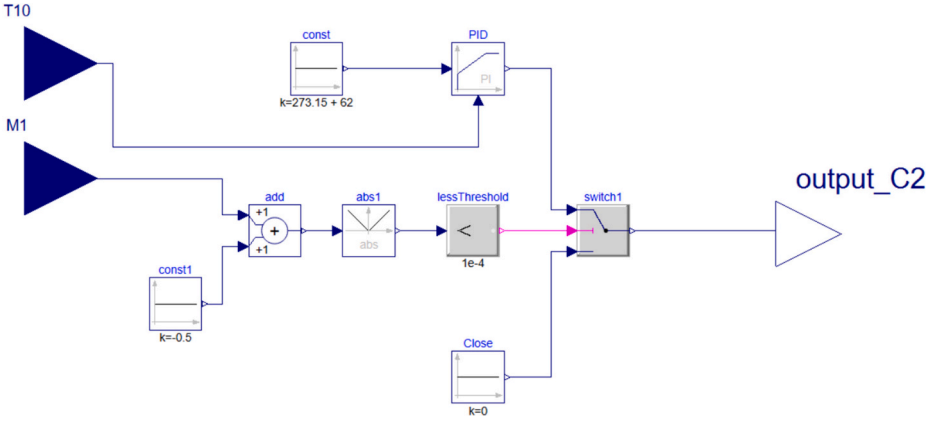

Fig. 9. C2 control block.

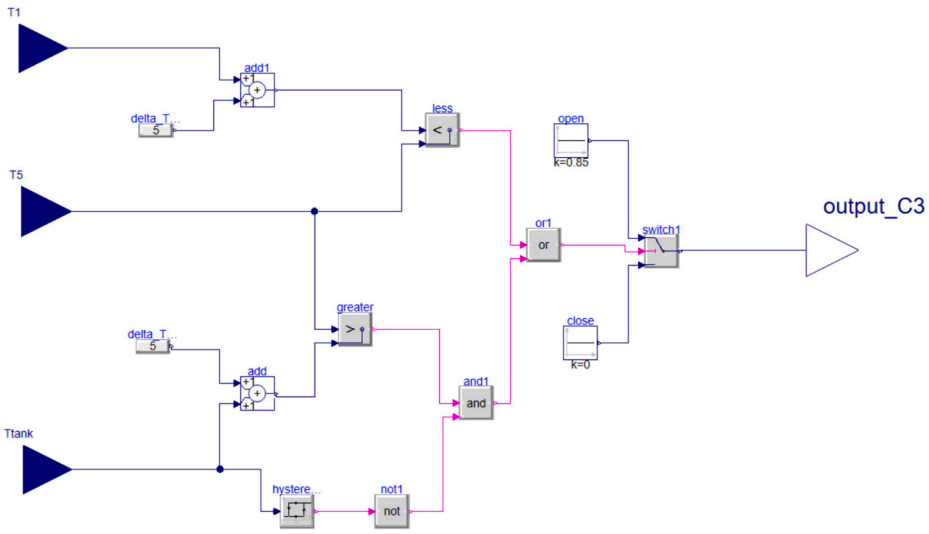

Fig. 10. C3 control block.

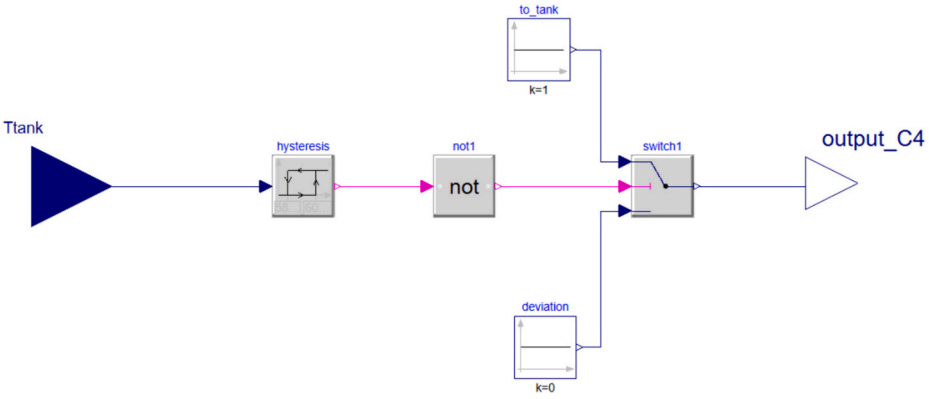

Fig. 11. C4 control block.

where Q_{annual} represents the estimated annual energy exchanged, Q_i is the energy exchanged during the i-th representative day, and N_i is the number of days in the year associated with that cluster, as reported in Table 2 and Table B1.

Fig. 13 schematically presents the main external inputs to the Dymola model and the key outputs used to assess the performance of the bidirectional substation.

2.4.3. Calculation and KPIs

For the comparative analysis of different test days, key performance indicators (KPIs) have been calculated on a daily basis. The analysis included self-consumption (S_C), which represents the percentage of locally produced thermal energy consumed on-site (Eq. 10); self-sufficiency (S_S), indicating how much thermal demand is satisfied by local production (Eq. 9); and the useful energy coefficient (U_{ec}), which reflects the percentage of locally generated thermal energy either consumed by the user or fed into the network (Eq. 11).

$$S_S = 100 \bullet \frac{E_{solar\ to\ DHW}}{E_{user\ load}} \tag{9}$$

$$S_C = 100 \bullet \frac{E_{solar\ to\ DHW}}{E_{solar}} \tag{10}$$

$$U_{ec} = 100 \bullet \frac{E_{solar\ to\ DHW} + E_{solar\ to\ DHN}}{E_{solar}} \tag{11}$$

where E_{solar} is the energy produced by solar plants, $E_{solar\ to\ DHN}$ is the energy produced by solar panels and fed into the network, $E_{solar\ to\ DHW}$ is the energy produced by solar panels for the end user DHW demand, and $E_{user\ load}$ is the thermal load for the end user.

3. Results and discussion

3.1. Trend of the main parameters

Figs. 14–17 illustrate key variables and parameters that demonstrate the proper functioning of the substation control systems, specifically those regulating the thermal power supplied from the DHN to the end-user. At this stage, the analysis focuses only on the network's contribution, temporarily excluding the solar input and the bidirectional energy feed into the DHN. Each figure displays, from top to bottom: the space heating hours; T_9 and T_{10}, representing the secondary circuit's return and supply temperatures, respectively; M_1 and M_{1p}, the flow rates controlled by valves V1 and V2, respectively; T_{tank}, which reflects the water temperature in the storage tank; and M8, the flow rate managed by the pump feeding the upper heat exchanger of the storage tank.

In all analyzed days, except for the summer day, the space heating schedule runs from 6:00 AM to 10:00 PM. During these hours, valve V1 (the on-off valve on primary circuit) is fully open, allowing M_1 to reach its nominal flow rate. This trend is evident across all figures, except for the summer configuration where heating is inactive. Notably, V1 also opens outside of these hours whenever the tank water temperature falls below its setpoint (60 °C with hysteresis of 2 °C). This occurs at the start

of the simulation, between 12:00 AM and around 2:00 AM, when the tank temperature is initialized at 20–25 °C, and again around 11:00 PM (with slight variations depending on the return temperature T9). To support the interpretation of these events, the corresponding time windows have been visually emphasized in the figures using semi-transparent light-blue bands, consistently across all four analyzed days. Notably, on the November day, no flow interruption is observed during the evening period, as a simultaneous DHW request causes a sharp drop in tank temperature, prompting the system to maintain the primary flow active beyond SH schedule.

Before reaching the HE1, M1 passes through valve V2, which is regulated by a PID controller. This controller monitors T_{10} and adjusts the flow to maintain T_{10} at its setpoint of 62 °C. When T_{10} approaches the setpoint, V2 partially closes, diverting some of the flow through a bypass. This behavior is particularly noticeable during the day of January, typically between 3:00 PM and 4:00 PM and again between 6:00 PM and 7:00 PM, where a decrease in M_{1p} coincides with T_{10} stabilizing at the setpoint. To support the interpretation of these events, the corresponding time windows have been visually emphasized in the figures using semi-transparent yellow bands. A different behavior is observed on the day of August, where, due to the absence of SH demand, the target temperature is reached more easily and the controller activates the bypass more promptly to limit the flow through HE1.

The M_8 flow rate, controlled by the pump feeding the upper heat exchanger of the storage tank, operates whenever the tank temperature drops below its setpoint of (60 °C with a 2 °C hysteresis). The adoption of the hysteresis effectively prevents excessive on/off cycling of the pump, contributing to the overall stability of the system. This is particularly evident in instances where T_{tank} rapidly approaches the activation threshold but remains within the hysteresis band, avoiding unnecessary pump activations. To illustrate this behavior, a specific moment has been highlighted with a light blue circle in both the January and August plots, where the tank temperature drops slightly below 60 °C but remains within the 2 °C hysteresis band, thus preventing the activation of the heat exchange.

A similar stabilizing effect of hysteresis is observed in the control of valve V1 on the primary side. While V1 fully opens during designated heating hours, it also responds to fluctuations in Ttank outside these periods. Such coordinated control strategies, leveraging hysteresis across both the primary and secondary circuits, ensure smooth system operation and efficient thermal management without introducing oscillatory behavior or energy inefficiencies. Overall, the control logic demonstrates robust performance across varying conditions, maintaining both the secondary circuit and storage tank temperatures within their respective thresholds. The interaction between V1, V1p, and the tank dynamics highlights the system's ability to adapt to fluctuating demands, ensuring stable operation throughout the different days analyzed.

Figs. 18–21 present key thermal power exchanges and variables critical for assessing the performance of the bidirectional substation. The figures illustrate how the implemented control logic regulates both energy input from the DHN and the solar energy utilization, while managing surplus energy feed into the network. Each figure displays, from top to bottom: the tank top temperature (Ttank top), referring to the top segment where the sensor is installed; the tank bottom temperature (Ttank bottom), useful for understanding the internal dynamics of the tank; the solar temperature sent to the tank (T5 to tank), activated when Ttank top drops below its setpoint; the solar temperature feed-in to the network (T6), measured after exchanging with or bypassing the tank and the nominal supply temperature from the DHN (T_1). This is followed by the DHW flow rate requested by the user and the thermal power exchanged through the three heat exchangers HE1, HE2, and HE3. These specific variables have been carefully selected as they are fundamental to understanding the system's dynamic behavior and the energy exchange among the different components.

Table 2
Test days characteristics.

Test days	Average daily T [°C]	Average daily radiation [W/m^2]	N° of days in the cluster
January 5	3.7	63	83
April 9	15.8	243	47
August 1	24.4	287	74
November 5	10.1	58	52

The thermal power dynamics across the heat exchangers are directly shaped by the implemented control strategies. Throughout all the analyzed days, HE1 plays a dominant role in charging the storage tank, while HE3 handles the reinjection of surplus heat back into the DHN. This behavior reflects the alignment of the system's operation with typical DHW demand patterns, which peak in the early morning and evening times when solar energy production is either negligible or completely absent. Solar contributions, intermittently reach temperatures sufficient to transfer heat to the tank, but these instances often align with periods of low DHW demand, when the tank temperature is already near its setpoint. As a result, opportunities to use solar energy for recharging the thermal storage are limited and occur only in short windows.

On day of January, for example, solar charging is confined to a brief period between 11:00 AM and just before 12:00 PM. This occurs when a DHW request causes the tank temperature to drop below its setpoint, while T5 remains sufficiently higher to enable thermal exchange. Thermal power is transferred through HE2, the heat exchanger connected to the solar loop, until the temperature difference drops, briefly interrupting the exchange, which resumes a few minutes after 12:00 PM as solar temperature increases. To support the interpretation of these events, the corresponding time window has been visually emphasized in the figure using a semi-transparent green band. Similarly, on day of April and August usable solar input occurs around 7:30 AM, between 8:30 AM and 9:00 AM. In these timeframes, early DHW request cause a drop in the tank top temperature, enabling thermal exchange with the solar loop through HE2. For the day of April, an additional charging phase also occurs shortly after 11:00 AM, when a smaller DHW demand briefly brings the tank temperature below its setpoint, again allowing thermal exchange with HE2. In contrast, on the November day, solar production remains very limited and occurs during periods when the tank is already at temperature, preventing any meaningful contribution to storage.

In all days, the tank temperature profile directly mirrors fluctuations in DHW demand, as each withdrawal of hot water by the user introduces cold water into the tank, causing sharp temperature drops. These variations are most pronounced during peak DHW usage periods, closely following the typical consumption patterns of the users. At the start of the simulation, the tank is initialized at 20 °C, which leads to a distinct charging phase in the early hours as the system works to reach the setpoint temperature. Over time, natural thermal losses contribute to gradual decreases in Ttank, further influenced by intermittent hot water demands throughout the day.

An additional layer of analysis concerns the interaction between Ttank top and Ttank bottom, the solar temperature directed to the tank (T5), and the DHW demand. The bottom section of the tank, where HE2 is located, naturally maintains lower temperatures compared to the top section, which contains the network-connected heat exchanger and functions as the DHW outlet zone. On the days of April and August, short periods in the early morning activate HE2, leading to a noticeable increase in Ttank bottom. These periods correspond to the green semi-transparent bands previously introduced in the figures to highlight the relevant time windows. This early solar preheating proves effective, as during subsequent DHW requests (e.g., around 11:00 AM), the introduction of cold water into the lower part of the tank has limited impact on Ttank top, which remains nearly constant in August and only slightly

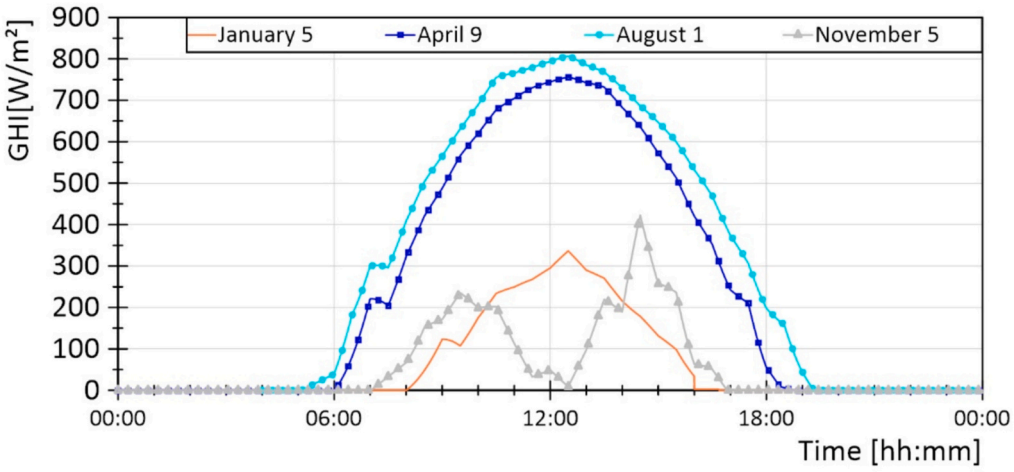

Fig. 12. Daily solar irradiation for the 4 selected days.

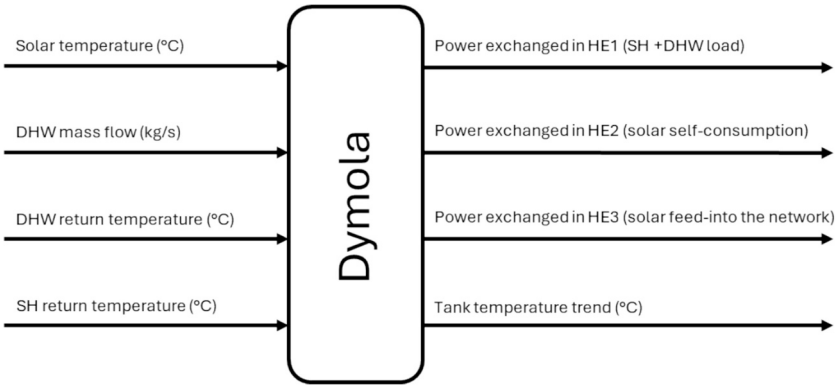

Fig. 13. External input and key output from Dymola model.

drops in April. Since the temperature sensor that controls thermal exchange with the tank is located in the top section, the system does not register a significant decrease and thus avoids activating additional charging from the network or the solar loop. In contrast, on the days of January and November, the absence of early morning solar charging keeps Ttank bottom at low temperatures, resulting in more pronounced drops in Ttank top during the first DHW demands. In January, however, a distinct solar charging phase takes place between 11:00 AM and 12:00 PM, causing a rapid increase in Ttank bottom. The lower part of the tank then stabilizes at a higher temperature and remains thermally charged for several hours. Later in the afternoon, during a DHW request shortly after 6:00 PM, Ttank bottom shows only a slight decrease, while Ttank top remains stable. November, by contrast, shows no exchange through HE2 at any point during the day. As a result, the bottom of the tank stays persistently cold, and each DHW request leads to a marked drop in the top temperature as highlighted by the yellow semi-transparent bands in the figures, which indicate the most critical request events. Overall, these observations show that even brief periods of localized solar charging in the lower tank region can help stabilize the temperature in the upper section, where control decisions are made. This results in fewer interventions from the network, especially in the hours following solar production.

These conditions highlight the efficiency of the bidirectional setup, as any surplus heat that cannot be stored in the tank is effectively fed into the network through HE3 when the solar temperature (T_6) surpasses the DHN supply temperature (T_1) by a sufficient ΔT. This reinjection is particularly significant during the summer day, when the DHN operates at a lower supply temperature (70 °C), allowing the solar collectors to more easily exceed this threshold and feed excess energy into the network.

Focusing on the thermal power exchanged in HE1, distinct patterns emerge depending on seasonal demand. On day of August, the power transfer through HE1 closely mirrors the fluctuations in T_{tank}, as there is no requirement for SH. Conversely, on the other days, SH demand significantly increases the thermal load on HE1, resulting in higher and more sustained power exchanges. This clear distinction highlights the substation's adaptability in responding to seasonal variations, efficiently balancing both SH and DHW needs. Furthermore, the bidirectional configuration enhances solar energy utilization and ensures effective management of surplus heat, maintaining optimal system performance throughout varying operational conditions.

Additionally, the rapid response of HE1 to temperature drops in the storage tank highlights the system's ability to maintain thermal stability even in the absence of space heating demand. On days with concurrent SH and DHW requirements, the power exchanged through HE1 demonstrates smooth modulation, indicating effective control strategies that prevent thermal overloads or inefficiencies. Furthermore, during transitional seasons, solar contributions can reduce the load on HE1, showcasing the substation's capability to dynamically balance renewable inputs with network supply.

3.2. Daily energy analysis

Figs. 22–24 illustrate the energy flows and key performance indicators (KPIs) for representative days of the four seasons. Specifically, Fig. 22 shows the breakdown of total user load between consumption for

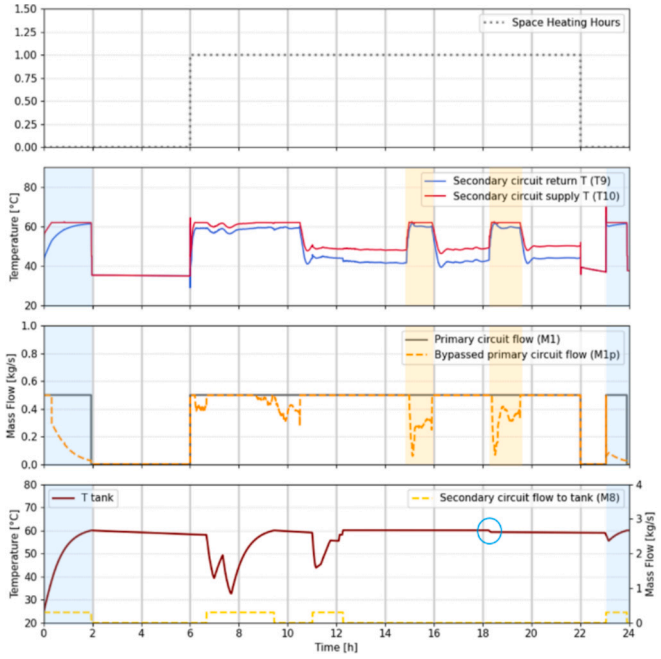

Fig. 14. Trend of the parameters regulating the thermal power supplied from the DHN to the end-user, January 5.

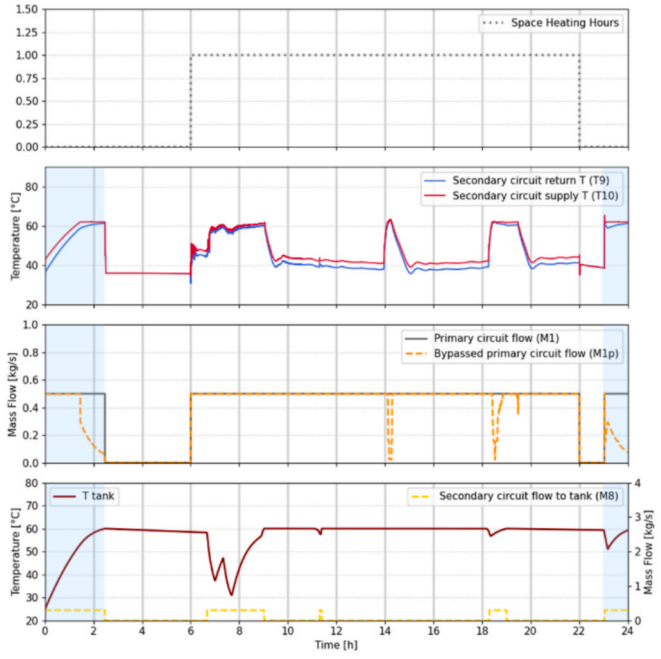

Fig. 15. Trend of the parameters regulating the thermal power supplied from the DHN to the end-user, April 9.

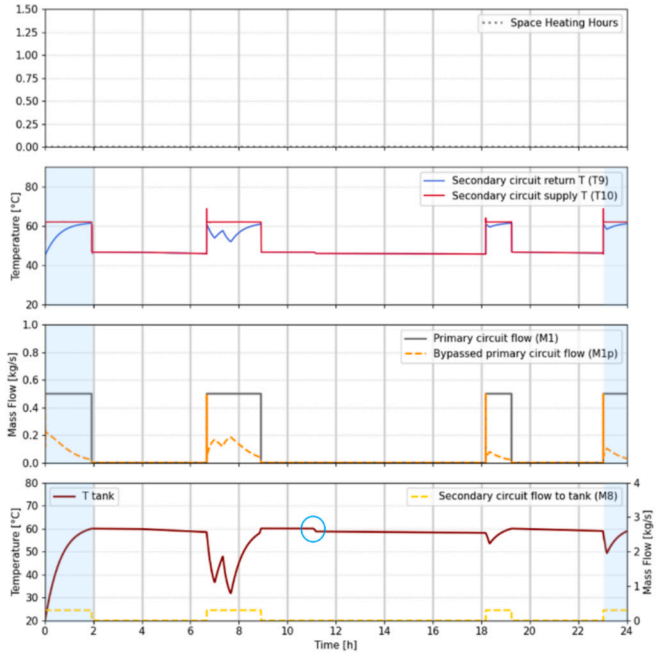

Fig. 16. Trend of the parameters regulating the thermal power supplied from the DHN to the end-user, August 1.

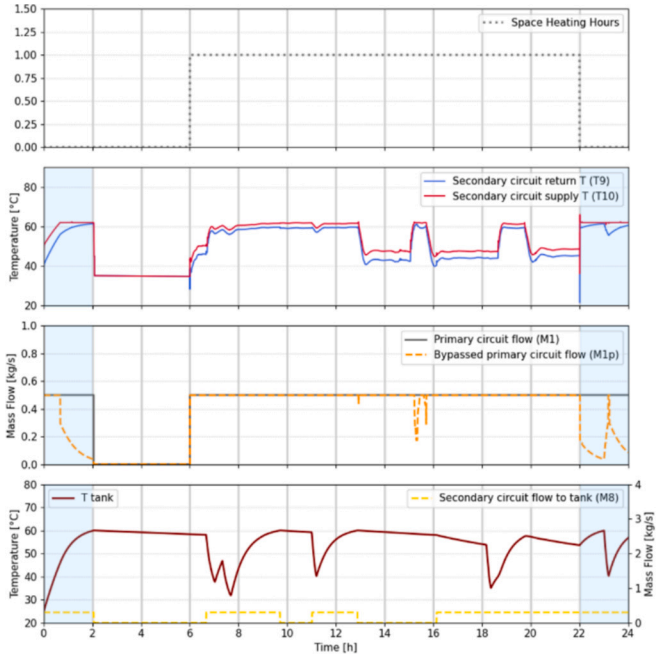

Fig. 17. Trend of the parameters regulating the thermal power supplied from the DHN to the end-user, November 5.

DHW and SH. The figure clearly shows that most of the energy demand is allocated to SH during the colder periods, with a sharp reduction in demand in the day of August when SH consumption drops to zero. The demand for DHW, however, remains steady between 40 and 45 kWh across all the simulated days, regardless of the season. The day in January records the highest demand for SH, consistent with the low temperatures observed on that day. On the other hand, the day in April shows the lowest demand, as it falls near the end of the heating season and corresponds to one of the warmest days.

Fig. 23 shows the breakdown of the total load for DHW and the self-sufficiency rate (S_S), indicating how much of the DHW demand is covered by solar energy. The DHW production, which occurs via the storage tank, is divided between the grid contribution through the upper heat exchanger and the contribution from the lower heat exchanger connected to the solar circuit. It is observed that most of the DHW demand is met by the grid, while solar energy contributes about 43 % during the days in April and January, 33 % on the August day, and provides no contribution on the November day.

Fig. 24 shows the total solar energy production and how it is used, with energy being divided between self-consumption for DHW and injection into the grid, thanks to the bidirectional configuration. This graph highlights the effectiveness of the bidirectional setup, which not

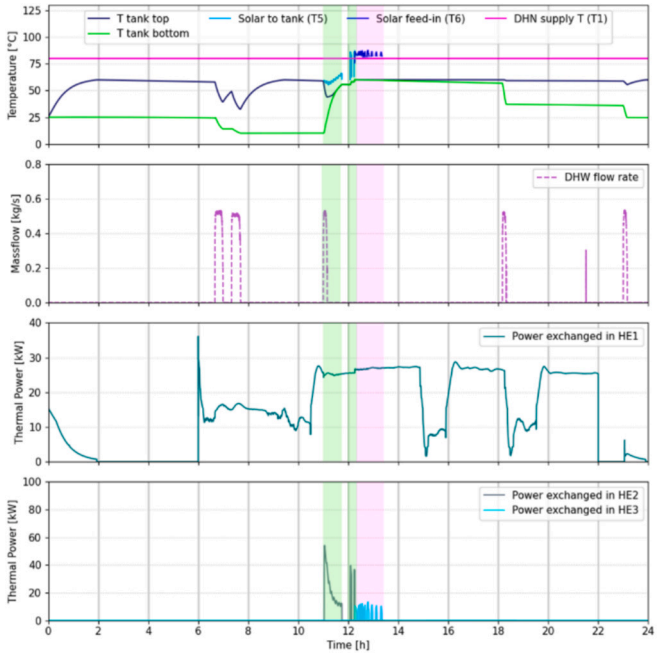

Fig. 18. Interaction between the HEs according to thermal demand and solar availability, January 5.

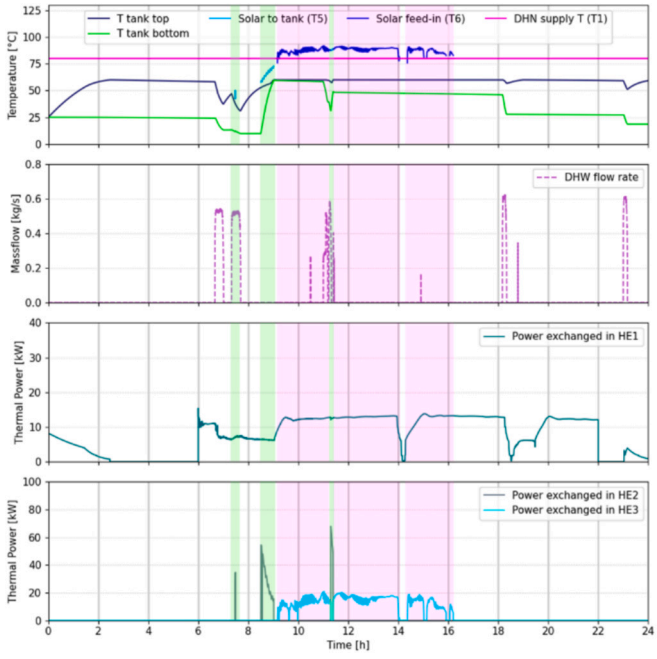

Fig. 19. Interaction between the HEs according to thermal demand and solar availability, April 9.

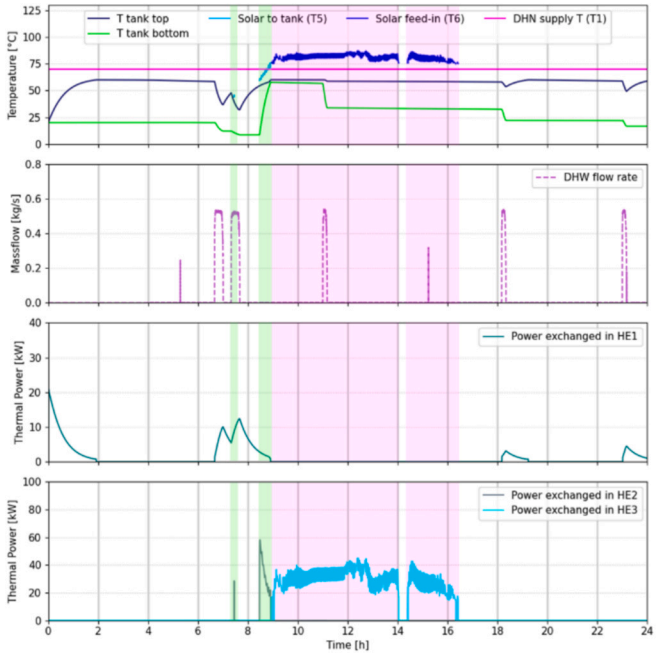

Fig. 20. Interaction between the HEs according to thermal demand and solar availability, August 1.

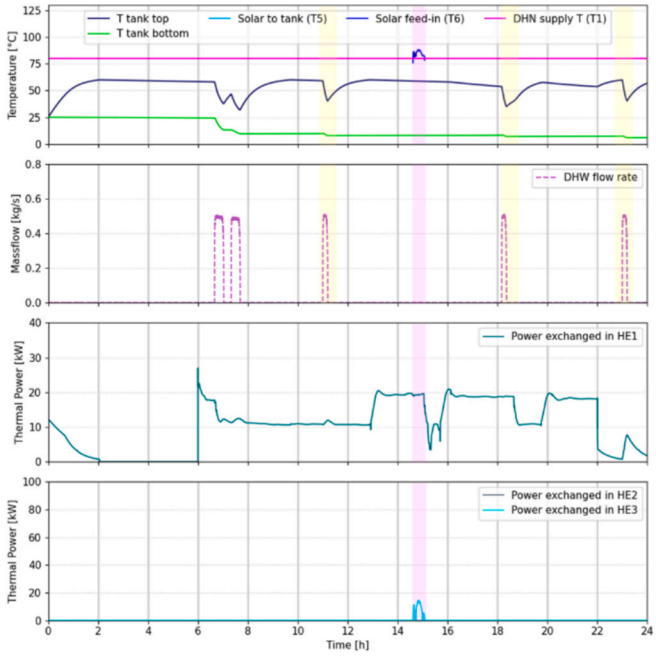

Fig. 21. Interaction between the HEs according to thermal demand and solar availability, November 5.

only meets internal energy demand but also optimizes the use of excess energy by feeding it into the network. The analysis uses the S_C coefficient to assess the portion of solar energy directly consumed by the user, and the Uec coefficient, which includes both the energy consumed internally and that fed into the grid, treating the latter as a valuable contribution to the overall system efficiency.

Since the control logic preserves the original behavior of the unidirectional substation, the solar panels first exchange energy with the tank for DHW production (if the tank temperature falls below the setpoint and there is sufficient solar temperature), and subsequently, if the remaining temperature is still sufficient for exchanging with the grid, the unused energy is fed into the network via HE3, thus prioritizing the unidirectional operation.

On the January day, despite low solar production, the system is able to utilize 47.3 % of the energy produced by the solar plant for self-consumption. With the bidirectional configuration, considering the useful effect of the energy fed into the network, the U_{ec} reaches to 60 %, demonstrating the system's ability to actively exchange unused thermal energy with the network. A similar trend is observed on the November day: no solar energy is used for direct self-consumption ($S_C = 0.1$ %), yet 25 % of the production is effectively recovered through the bidirectional

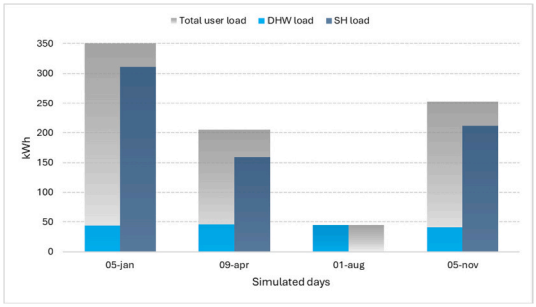

Fig. 22. User thermal load split between space heating and domestic hot water.

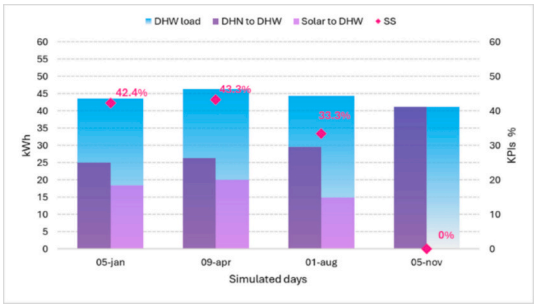

Fig. 23. DHW thermal load supplied by district heating and solar system, and corresponding self-sufficiency rate.

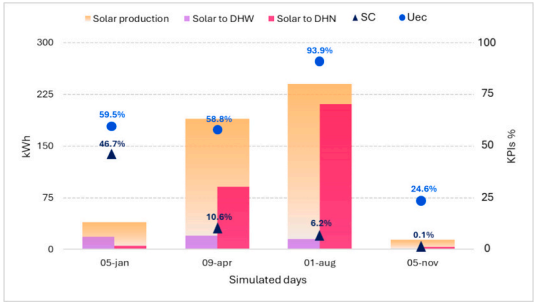

Fig. 24. Distribution of solar energy between DHW self-consumption and grid feed-in, with analysis of the self-consumption rate and useful coefficient.

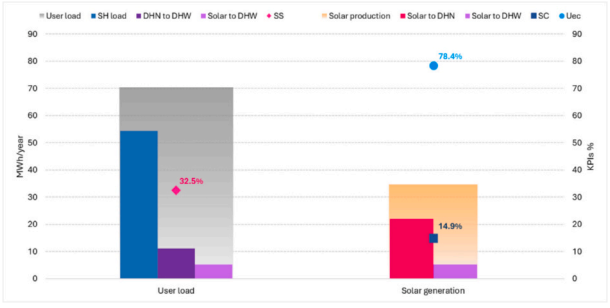

Fig. 25. Energy flows resulting from annual extrapolation.

setup. This highlights how the mismatch between generation and demand significantly reduces self-consumption. The benefits of the bidirectional configuration become even more evident on the April and August days. On the April day, self-consumption is limited to 10.6 %, while the U_{ec} rises to 58.8 %. The most notable improvement, however, occurs on the August day: only 6.2 % of the solar energy is self-consumed, but the bidirectional configuration enables the effective use of 94 % of the generated energy. This outstanding result is not only due to higher solar irradiance, but also to the reduction in DHN flow temperature from 80 °C to 70 °C, which broadens the temperature range suitable for feeding excess thermal energy into the grid.

In conclusion, the bidirectional configuration proves highly effective in maximizing the use of solar energy, especially on high-production days, minimizing losses, and enhancing excess energy through integration with the DHN.

3.3. Annual extrapolation results

The daily results for the two additional representative days used to support the reliability of the annual extrapolation are provided in Appendix B (Figs. B1–B4). Fig. 25 summarizes the annual energy flows and KPIs obtained through the extrapolation methodology described in Section 2.4.2. On the left side, the total thermal demand of the user is shown, including SH and DHW load, the latter being covered both by the DHN and by the local solar thermal system. On the right, the annual solar energy production is detailed, distinguishing between the share used locally for DHW heating and the amount fed into the network, enabled by the bidirectional configuration of the substation.

The annual S_S rate, calculated with respect to the DHW load, is 32.5 %, in line with the result observed in the daily analysis in Section 3.1, where DHW demand often causes a drop in T_{tank} during hours when solar energy is either unavailable or too weak to activate heat exchange. The relatively low annual S_C rate of 14.9 % is mainly due to the lack of overlap between solar production and thermal demand. In many cases, solar energy becomes available when the tank, especially its upper part ($T_{tank\ top}$) where control decisions are triggered, is already close to the setpoint temperature, making further charging ineffective. While early solar charging of the bottom tank layer ($T_{tank\ bottom}$) contributes to thermal stratification and can mitigate later DHW demand, its impact on improving self-consumption remains limited.

However, when considering also the share of solar energy that is fed into the DHN through the bidirectional setup, the annual U_{ec} is equal to 78.4 %. This clearly demonstrates the added value of the prosumer-oriented approach: instead of wasting surplus solar energy that cannot be stored locally, the system can feed it back into the DHN for potential downstream use. This approach helps overcome the limitations of conventional unidirectional systems, which depend entirely on local self-consumption and are often limited by the mismatch between production and demand, as well as by fixed tank temperature thresholds.

Although summer conditions contribute most to the amount of energy fed into the network, largely due to the reduced DHN supply temperature (70 °C) which facilitates solar feed-in, the annual data also indicates that the bidirectional setup enables a meaningful export of solar energy even during colder periods. This confirms the effectiveness of the retrofit solution, highlighting its potential not only under peak production conditions but also during less favourable seasons.

Overall, the bidirectional substation configuration proves to be a robust and replicable strategy to maximize the exploitation of distributed solar heat production. By leveraging both local consumption and network feed-in, it ensures that a large share of the available renewable energy is effectively utilized within the system, enhancing both energy efficiency and operational flexibility.

3.4. Network level consideration

It should be considered that solar thermal production often peaks, especially around midday—when the thermal demand from other users is low or even null. This condition could potentially lead to overheating or inefficient operation. In this regard, the introduction of solar thermal energy into the return circuit helps mitigate the risk of overheating by mixing with the cooler return water. Naturally, this results in an increase in the return temperature to the generation plant, which is particularly

undesirable when a CHP unit is operating. However, CHP systems are typically turned off during spring and summer, when solar production is higher. Under these conditions, the DHN can act as an additional thermal buffer, absorbing excess solar energy when user demand is low or absent. While this approach implies accepting some thermal losses in the network, the overall energy balance favors a greater exploitation of renewable heat. The supply-to-return configuration minimizes the distance traveled by the injected solar energy, especially when there is no concurrent demand from other users—thus reducing thermal dispersion. Moreover, the control logic implemented in the bidirectional substation prioritizes local thermal storage charging and only activates feed-in to the DHN when the tank is fully charged. This strategy further minimizes losses and helps prevent overheating. These findings confirm that, even during low-demand periods, the proposed retrofit ensures safe and efficient operation while enhancing the overall utilization of renewable heat. Future work could explore the cumulative impact of multiple prosumer substations feeding into the network simultaneously, particularly under low-demand conditions, to assess potential effects on return temperature and overall system balance.

4. Conclusion

Decarbonizing the heating and cooling sector is essential for reducing dependence on fossil fuels, with DHN playing a key role in integrating RES and WH. In this context, decentralized solutions at the thermal substation level provide significant opportunities to optimize efficiency and enhance the operational flexibility of DHN. These solutions support the integration of thermal prosumers and encourage their active participation in the decarbonization process.

An innovative retrofit design for an existing substation has been proposed, enabling the bidirectional exchange of thermal energy and allowing excess solar energy to be fed into the network. The design was based on a real DHN in the city of Turin, whose technical and spatial constraints were carefully considered to ensure the solution's replicability without requiring deep interventions. Through a non-invasive approach, the original operational integrity of the infrastructure has been preserved, adding minimal new components and implementing a control system that enhances the use of renewable energy without altering the existing system's operation. To validate the feasibility of the proposed solution under realistic operating conditions, an experimental prototype was adapted to replicate the retrofit configuration. This setup enabled the acquisition of high-resolution input data such as real thermal loads and solar production profiles which were then used for the numerical model to perform dynamic simulations closely aligned with actual system behavior.

The results from dynamic simulations, performed using Modelica language and Dymola software, demonstrate the effectiveness of the bidirectional substation. The control system proved capable of efficiently regulating the thermal energy exchange under different seasonal and demand conditions.

In general, during spring and summer days, only a small portion of the solar energy produced is used to meet DHW demand, with self-consumption rates of 10.6 % and 6.2 %, respectively. In contrast, during the winter day, a significantly higher self-consumption rate is observed (47.3 %). This highlights how, despite the available solar energy during the warmer days, it is not fully utilized due to the temporal mismatch between peak solar production and periods of high DHW demand. Specifically, the daily solar energy used to meet the DHW needs ranges between 15 and 20 kWh across all days, except for the autumn day, where low solar production, combined with a moment of low demand, contributes nothing to satisfying the energy needs.

The proposed bidirectional configuration allows for the recovery of much of the unused solar energy by feeding it into the network through the return branch. This results in the utilization of 60 % of the solar energy produced during the spring day and 93.9 % during the summer day. The latter outcome is also facilitated by the lowering of the network's supply temperature in the summer months, from 80 °C to 70 °C, enabling the use of a wider temperature range for thermal energy exchange. Moreover, the substation's ability to exchange energy with the network, even during periods of low solar production, further underscores the benefits of the retrofit, ensuring a more efficient and flexible energy management system. To evaluate the substation's performance over an entire year, an extrapolation method validated in the literature was applied by simulating additional representative days, enabling a reliable annual assessment while keeping computational effort within reasonable limits. The results confirmed the benefits of the bidirectional setup, with an annual self-consumption rate of 14.9 % and a total use of solar energy reaching 78.4 % when including the energy fed into the network. This result was largely influenced by summer conditions, where increased solar production, reduced DHN supply temperatures, and the mismatch between generation and demand facilitated greater feed-in of surplus heat to the network.

The results obtained for this substation, based on an existing infrastructure, show that the proposed bidirectional configuration can be easily replicated in similar contexts, particularly in Italy, where many district heating networks serve residential customers for DHW and SH. This solution is particularly applicable in Northern Italy, where DHN is widespread, and the configurations of substations are generally homogeneous.

Future studies could focus on analyzing the effects of integrating a larger number of thermal prosumers into the network, exploring the implications for energy management and operational efficiency. A key area of interest would be the management of the return temperature increase, examining how the heating plants could respond to such a rise while maintaining an optimal balance between heat demand and network capacity, preventing the risk of overload, and improving the overall system efficiency.

Funding acknowledgements

This research was funded in the Program Agreement between the Italian National Agency for New Technologies, Energy and Sustainable Economic Development (ENEA) and the Ministry of Environment and Energy Security (MASE) for the Electric System Research, in the framework of its Implementation Plan for 2022–2024, Project 1.5 "High-efficiency buildings for the energy transition" (CUP I53C22003050001), Work Package 3 "Innovative technologies and components for increasing the energy performance of buildings".

CRediT authorship contribution statement

Federico Gianaroli: Writing – original draft, Visualization, Software, Methodology, Investigation, Formal analysis, Conceptualization. **Mattia Ricci:** Writing – review & editing, Visualization, Software, Project administration, Methodology, Conceptualization. **Paolo Sdringola:** Writing – review & editing, Project administration, Investigation, Conceptualization. **Mauro Pipiciello:** Writing – review & editing, Visualization, Investigation. **Diego Menegon:** Writing – review & editing, Visualization. **Francesco Melino:** Supervision.

Declaration of competing interest

The authors declare that they have no known competing financial interests or personal relationships that could have appeared to influence the work reported in this paper.

Appendix A. Appendix

Fig. A1. DHN schematic overview [12].

Appendix B. Appendix

Table B1
Characteristics of test days added for annual extrapolation.

Test days	Average daily T [°C]	Average daily radiation [W/m^2]	N° of days in the cluster
March 21	9.9	156	42
May 24	20.1	153	67

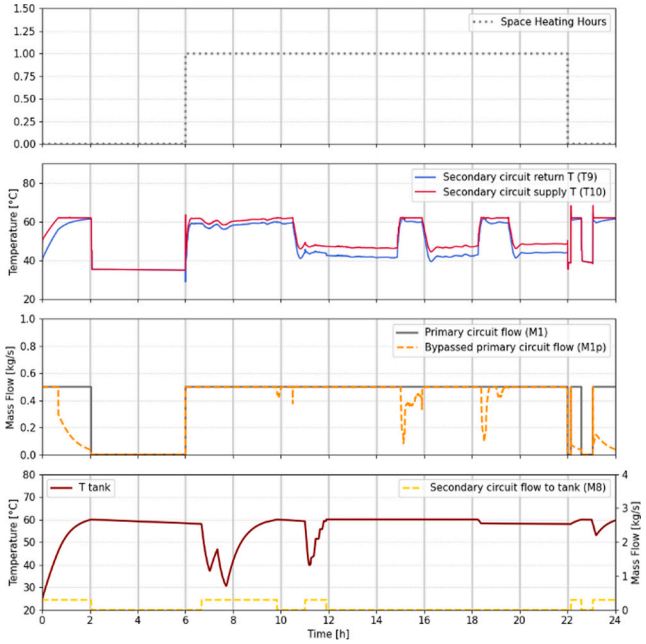

Fig. B1. Trend of the parameters regulating the thermal power supplied from the DHN to the end-user, March 21.

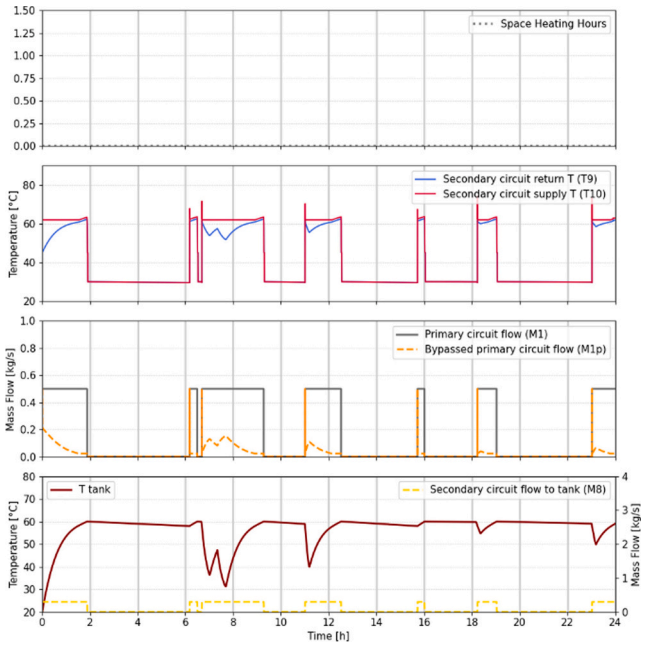

Fig. B2. Trend of the parameters regulating the thermal power supplied from the DHN to the end-user, May 24.

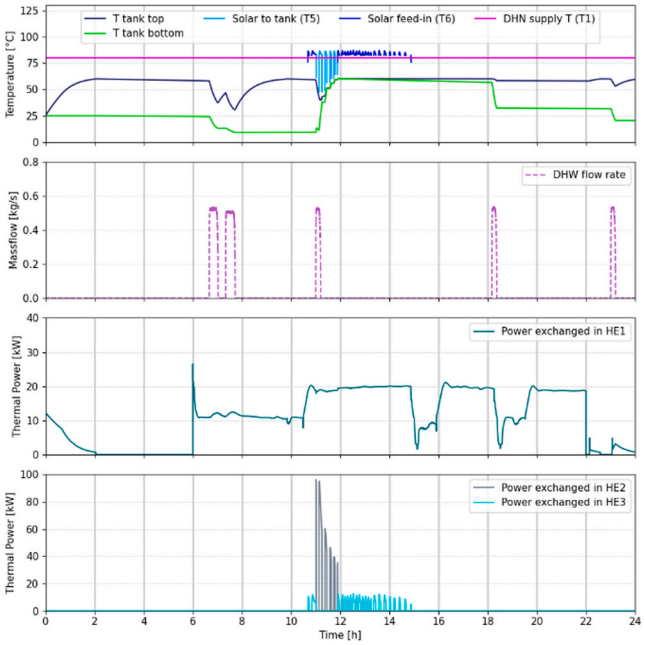

Fig. B3. Interaction between the HEs according to thermal demand and solar availability, March 21.

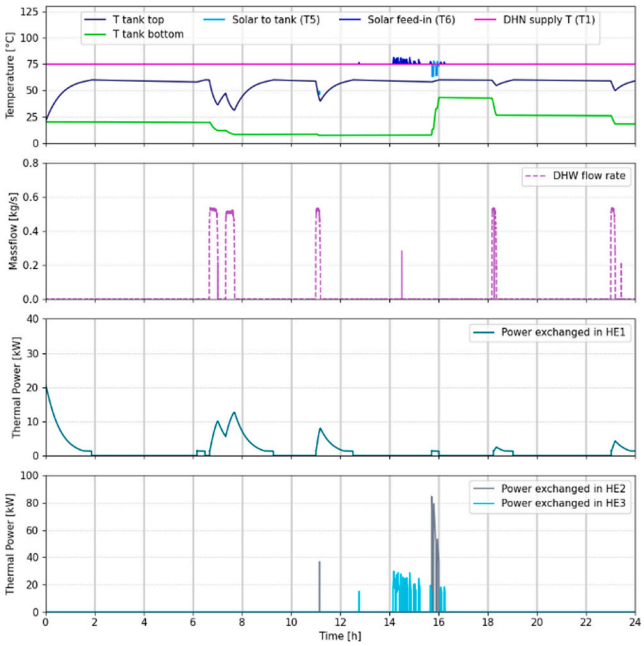

Fig. B4. Interaction between the HEs according to thermal demand and solar availability, May 24.

Data availability

Data will be made available on request.

References

[1] European Climate Law - European Commission. Available online: https://climate.ec.europa.eu/eu-action/european-climate-law_en; 2025. accessed on 8 July 2024.

[2] Difs K. National Energy Policies: obstructing the reduction of global CO2 emissions? An analysis of Swedish energy policies for the district heating sector. Energy Policy 2010;38:7775–82. https://doi.org/10.1016/j.enpol.2010.08.037.

[3] Billerbeck A, Breitschopf B, Preuß S, Winkler J, Ragwitz M, Keles D. Perception of district heating in Europe: a deep dive into influencing factors and the role of regulation. Energy Policy 2024;184:113860. https://doi.org/10.1016/j.enpol.2023.113860.

[4] Eurostat. Available online: https://ec.europa.eu/eurostat/statistics-explained/index.php?title=Renewable_energy_statistics; 2025. accessed on 28 March 2023.

[5] Energy Efficiency Directive. Available online: https://energy.ec.europa.eu/topics/energy-efficiency/energy-efficiency-targets-directive-and-rules/energy-efficiency-directive_en. accessed on 9 July 2024.

[6] Bürger V, Steinbach J, Kranzl L, Müller A. Third party access to district heating systems - challenges for the practical implementation. Energy Policy 2019;132:881–92. https://doi.org/10.1016/j.enpol.2019.06.050.

[7] Connolly D, Lund H, Mathiesen BV, Werner S, Möller B, Persson U, et al. Heat roadmap Europe: Combining District heating with heat savings to decarbonise the EU energy system. Energy Policy 2014;65:475–89. https://doi.org/10.1016/j.enpol.2013.10.035.

[8] District Heating Systems: Uneven Use Around the World. Available online: https://www.planete-energies.com/en/media/article/district-heating-systems-uneven-use-around-world; 2025. accessed on 25 July 2024.

[9] AIRU Archives. Available online: https://www.airu.it/tag/annuario/; 2025. accessed on 17 February 2025.

[10] Directive (EU) 2018/2001 of the European Parliament and of the Council of 11 December 2018 on the Promotion of the Use of Energy from Renewable Sources (Recast) (Text with EEA Relevance). vol. 328; 2018.

[11] Gianaroli F, Preziosi M, Ricci M, Sdringola P, Ancona MA, Melino F. Exploring the academic landscape of energy communities in Europe: a systematic literature review. J Clean Prod 2024;451:141932. https://doi.org/10.1016/j.jclepro.2024.141932.

[12] Dattilo A, Melino F, Ricci M, Sdringola P. Optimizing thermal energy sharing in Smart District heating networks. Energies 2024;17. https://doi.org/10.3390/en17122936.

[13] Ancona MA, Bianchi M, Branchini L, De Pascale A, Melino F, Peretto A, et al. Influence of the prosumer allocation and heat production on a district heating network. Front Mech Eng 2021;7. https://doi.org/10.3389/fmech.2021.623932.

[14] Gianaroli F, Ricci M, Sdringola P, Alessandra Ancona M, Branchini L, Melino F. Development of dynamic sharing keys: algorithms supporting Management of Renewable Energy Community and Collective Self Consumption. Energ Build 2024;311. https://doi.org/10.1016/j.enbuild.2024.114158.

[15] Bachmann M, Fürst Y, Stanica D, Kriegel M. dhcSim — a Modelica library for simple modeling of complex DHC systems. Energy Rep 2021;7:294–303. https://doi.org/10.1016/j.egyr.2021.08.143.

[16] Stanica D-I, Bachmann M, Kriegel M. Design and performance of a multi-level Cascading District heating network with multiple prosumers and energy storage. Energy Rep 2021;7:128–39. https://doi.org/10.1016/j.egyr.2021.08.163.

[17] Testasecca T, Catrini P, Beccali M, Piacentino A. Dynamic simulation of a 4th Generation District heating network with the presence of prosumers. Energy Convers Manage: X 2023;20. https://doi.org/10.1016/j.ecmx.2023.100480.

[18] Brand L, Calvén A, Englund J, Landersjö H, Lauenburg P. Smart District heating networks – a simulation study of prosumers' impact on technical parameters in distribution networks. Appl Energy 2014;129:39–48. https://doi.org/10.1016/j.apenergy.2014.04.079.

[19] Brange L, Englund J, Lauenburg P. Prosumers in district heating networks – a Swedish case study. Appl Energy 2016;164:492–500. https://doi.org/10.1016/j.apenergy.2015.12.020.

[20] Dibos S, Pesch T, Benigni A. HeatNetSim: an open-source simulation tool for heating and cooling networks suitable for future energy systems. Energy 2024;312:133588. https://doi.org/10.1016/j.energy.2024.133588.

[21] Lickleder T, Zinsmeister D, Lukas L, Speer F, Hamacher T, Perić VS. Control of bidirectional prosumer substations in smart thermal grids: a weighted proportional-integral control approach. Appl Energy 2024;354. https://doi.org/10.1016/j.apenergy.2023.122239.

[22] Gross M, Karbasi B, Reiners T, Altieri L, Wagner H-J, Bertsch V. Implementing prosumers into heating networks. Energy 2021;230:120844. https://doi.org/10.1016/j.energy.2021.120844.

[23] Kauko H, Kvalsvik KH, Rohde D, Nord N, Utne Å. Dynamic modeling of Local District heating grids with prosumers: a case study for Norway. Energy 2018;151:261–71. https://doi.org/10.1016/j.energy.2018.03.033.

[24] Wang D, Carmeliet J, Orehounig K. Design and assessment of district heating systems with solar thermal prosumers and thermal storage. Energies 2021;14. https://doi.org/10.3390/en14041184.

[25] Lichtenegger K, Wöss D, Halmdienst C, Höftberger E, Schmidl C, Pröll T. Intelligent heat networks: first results of an energy-information-cost-model. Sustain Energy, Grids Networks 2017;11:1–12. https://doi.org/10.1016/j.segan.2017.05.001.

[26] Martinazzoli G, Pasinelli D, Lezzi AM, Pilotelli M. Design of a 5th Generation District heating substation prototype for a real case study. Sustainability (Switzerland) 2023;15. https://doi.org/10.3390/su15042972.

[27] Sdringola P, Ricci M, Ancona MA, Gianaroli F, Capodaglio C, Melino F. Modelling a prototype of bidirectional substation for district heating with thermal prosumers. Sustainability 2023;15:4938. https://doi.org/10.3390/su15064938.

[28] Pipiciello M, Caldera M, Cozzini M, Ancona MA, Melino F, Di Pietra B. Experimental characterization of a prototype of bidirectional substation for district heating with thermal prosumers. Energy 2021;223:120036. https://doi.org/10.1016/j.energy.2021.120036.

[29] Dino GE, Catrini P, Palomba V, Frazzica A, Piacentino A. Promoting the flexibility of thermal prosumers equipped with heat pumps to support power grid

management. Sustainability (Switzerland) 2023;15. https://doi.org/10.3390/su15097494.
[30] Zinsmeister D, Licklederer T, Christange F, Tzscheutschler P, Perić VS. A comparison of prosumer system configurations in district heating networks. Energy Rep 2021;7:430–9. https://doi.org/10.1016/j.egyr.2021.08.085.
[31] Rosemann T, Löser J, Rühling K. A new DH control algorithm for a combined supply and feed-in substation and testing through hardware-in-the-loop. Energy Procedia 2017;116:416–25. https://doi.org/10.1016/j.egypro.2017.05.089.
[32] Lamaison N, Bavière R, Cheze D, Paulus C. A multi-criteria analysis of bidirectional Solar District heating substation architecture. In: Proceedings of the proceedings of SWC2017/SHC2017. Abu Dhabi: International Solar Energy Society; 2017. p. 1–11.
[33] Lamaison N, Cheze D, Robin J-F, Bruyat F, Lefrancois F. Operational behaviour of a solar-fed bidirectional substation for 4GDH networks. In: Proceedings of the proceedings of the ISES solar world congress 2021. International Solar Energy Society: Virtual; 2021. p. 1–10.
[34] Pipiciello M, Trentin F, Soppelsa A, Menegon D, Fedrizzi R, Ricci M, et al. The bidirectional substation for district heating users: experimental performance assessment with operational profiles of prosumer loads and distributed generation. Energ Build 2024;305:113872. https://doi.org/10.1016/j.enbuild.2023.113872.
[35] Sdringola P, Pipiciello M, Ricci M, Gianaroli F, Menegon D, Trentin F, et al. Prosumers and district heating: experimental validation of strategies to improve thermal energy production and consumption. Energ Build 2025;338:115713. https://doi.org/10.1016/j.enbuild.2025.115713.
[36] Gianaroli F, Pipiciello M, Sdringola P, Trentin F, Ricci M, Di Pietra B, et al. Empowering prosumers in district heating networks: experimental analysis and performance evaluation of a bidirectional substation2; 2024. p. 1188–99.
[37] Höffner D, Glombik S. Energy system planning and analysis software—a comprehensive Meta-review with special attention to urban energy systems and district heating. Energy 2024;307. https://doi.org/10.1016/j.energy.2024.132542.
[38] Abugabbara M, Javed S, Bagge H, Johansson D. Bibliographic analysis of the recent advancements in modeling and co-simulating the fifth-Generation District heating and cooling systems. Energ Build 2020;224:110260. https://doi.org/10.1016/j.enbuild.2020.110260.
[39] Buildings.Fluid.Storage.StratifiedEnhancedInternalHex. Available online: https://build.openmodelica.org/Documentation/Buildings.Fluid.Storage.StratifiedEnhancedInternalHex.html. accessed on 28 April 2025.
[40] Meteonorm. Available online: https://meteonorm.com/; 2025. accessed on 22 July 2025.
[41] El-Baz W, Mayerhofer L, Tzscheutschler P, Wagner U. Hardware in the loop real-time simulation for heating systems: model validation and dynamics analysis. Energies 2018;11:3159. https://doi.org/10.3390/en11113159.
[42] Development of Systemic Packages for Deep Energy Renovation of Residential and Tertiary Buildings Including Envelope and Systems | FP7. 2025.
[43] Jordan U, Vajen K. DHWcalc: Program to generate domestic hot water profiles with statistical means for user defined conditions. 2005.
[44] Oekotech-GS DatenEnergyLabel - AIT_20151016. Available online: http://www.oekotech.biz/UserFiles/File/DownloadFiles/oekotech-GS%20DatenEnergyLabel%20-%20AIT_20151016.pdf; 2025. accessed on 22 July 2025.
[45] Menegon D, Soppelsa A, Fedrizzi R. Clustering methodology for defining a short test sequence for whole system testing of solar and heat pump systems. In: Proceedings of the proceedings of SWC2017/SHC2017. Abu Dhabi: International Solar Energy Society; 2017. p. 1–11.